Acta Biomaterialia xxx (xxxx) xxx

Contents lists available at ScienceDirect

Acta Biomaterialia

journal homepage: www.elsevier.com/locate/actbio

Full length article

Quantifying physical degradation alongside recording and stimulation performance of 980 intracortical microelectrodes chronically implanted in three humans for 956-2130 days

David A. Bjånes [a,q,*], Spencer Kellis [b], Robert Nickl [c], Brian Baker [d], Tyson Aflalo [a], Luke Bashford [e], Srinivas Chivukula [f], Matthew S. Fifer [g], Luke E. Osborn [h], Breanne Christie [g], Brock A. Wester [g], Pablo A. Celnik [i], Daniel Kramer [j], Kelsie Pejsa [a], Nathan E. Crone [k], William S. Anderson [l], Nadar Pouratian [m], Brian Lee [b,n], Charles Y. Liu [b,n,p], Francesco V. Tenore [g,1], Loren Rieth [o,1], Richard A. Andersen [a,q,1]

[a] Department of Biology and Biological Engineering, California Institute of Technology, Pasadena, CA, USA
[b] Department of Neurological Surgery, Keck School of Medicine of USC, Los Angeles, CA 90033, USA
[c] Department of Physical Medicine and Rehabilitation, Johns Hopkins University School of Medicine, Baltimore, MD, USA
[d] Electrical and Computer Engineering Univ. of Utah, Salt Lake City, UT, USA
[e] Faculty of Medical Sciences, Newcastle University, Newcastle upon Tyne, UK
[f] Department of Neurosurgery, Kaiser Permanente Los Angeles Medical Center, Los Angeles, CA 90027, USA
[g] Research and Exploratory Development Department, Johns Hopkins University Applied Physics Laboratory, Laurel, MD, 20723, USA
[h] Department of Biomedical Engineering, Case Western Reserve University, Cleveland, OH, 44106, USA
[i] Shirley Ryan AbilityLab, Chicago, Il, 60611, USA
[j] Department of Neurological Surgery, University of Colorado Hospital, CO, 80045, USA
[k] Department of Neurology, Johns Hopkins University School of Medicine, Baltimore, MD, 21287 USA
[l] Department of Neurosurgery, Johns Hopkins University School of Medicine, Baltimore, MD, 21287, USA
[m] Department of Neurological Surgery, UT Southwestern Medical Center, Dallas, TX 75390, USA
[n] USC Neurorestoration Center, Department of Neurological Surgery, Keck School of Medicine of USC, Los Angeles, CA 90033, USA
[o] Mechanical, Materials, and Aerospace Engineering, West Virginia University, Morgantown, WV, USA
[p] Rancho Los Amigos National Rehabilitation Center, Downey, CA, USA
[q] Tianqiao and Chrissy Chen Institute for Neuroscience, CA, USA

ARTICLE INFO

Keywords:
Electrode
Scanning electron microscopy
Intra-cortical
Brain computer interface

ABSTRACT

The clinical success of brain computer interfaces (BCI) depends on overcoming both biological and material challenges to ensure a long-term stable connection for neural recording and stimulation. This study systematically quantified damage that microelectrodes sustained during chronical implantation in three people with tetraplegia for 956–2130 days. Using scanning electron microscopy (SEM), we imaged 980 microelectrodes from eleven Neuroport arrays tipped with platinum (Pt, $n = 8$) and sputtered iridium oxide film (SIROF, $n = 3$). Arrays were implanted/explanted from posterior parietal, motor and somatosensory cortices across three clinical sites (Caltech/UCLA, Caltech/USC, APL/Johns Hopkins). From the electron micrographs, we quantified and correlated physical damage with functional outcomes measured *in vivo*, prior to explant (recording quality, noise, impedance and stimulation ability).

Despite greater physical degradation, SIROF electrodes were twice as likely to record neural activity than Pt (measured by SNR). For SIROF, 1 kHz impedance significantly correlated with all physical damage metrics, recording metrics, and stimulation performance, suggesting a reliable measurement of *in vivo* degradation. We observed a new degradation type, primarily on stimulated electrodes ("pockmarked" vs "cracked") electrodes; however, no significant degradation due to stimulation or amount of charge delivered. We hypothesize erosion of the silicon shank accelerates damage to the electrode / tissue interface, following damage to the tip metal.

* Corresponding author at: California Institute of Technology, 1200 E California Blvd, Pasadena, CA, USA.
E-mail address: dbjanes@caltech.edu (D.A. Bjånes).
[1] Senior authors

https://doi.org/10.1016/j.actbio.2025.02.030
Received 27 September 2024; Received in revised form 7 February 2025; Accepted 11 February 2025
Available online 2 March 2025

These findings link quantitative measurements to the microelectrodes' physical condition and their capacity to record/stimulate. These data could lead to improved manufacturing processes or novel electrode designs to improve long-term performance of BCIs, making them vitally important as multi-year clinical trials of BCIs are becoming more common.

Statement of significance: Long-term performance stability of the electrode-tissue interface is essential for clinical viability of brain computer interface (BCI) devices; currently, materials degradation is a critical component for performance loss. Across three human participants, ten micro-electrode arrays (plus one control) were implanted for 956–2130 days. Using scanning electron microscopy (SEM), we analyzed degradation of 980 electrodes, comparing two types of commonly implanted electrode tip metals: Platinum (Pt) and Sputtered Iridium Oxide Film (SIROF). We correlated observed degradation with *in vivo* electrode performance: recording (signal-to-noise ratio, noise, impedance) and stimulation (evoked somatosensory percepts). We hypothesize penetration of the electrode tip by biotic processes leads to erosion of the supporting silicon core, which then accelerates further tip metal damage. These data could lead to improved manufacturing processes or novel electrode designs towards the goal of a stable BCI electrical interface, spanning a multi-decade participant lifetime.

1. Introduction

Long-term recording and stimulation stability of microelectrode arrays is a fundamental requirement for the clinical viability of intracortical brain computer interfaces (BCIs). Such BCI devices hold great promise for use in therapeutic and restoration applications by recording cortical neural activity [1]. These signals can be processed to decode an extraordinary amount of detailed information: motor planning and intent [2–10], high-level cognitive goals [11,12], speech and language [13,14], and dysregulated neural activity [15]. Furthermore, BCI's can write information into cortical networks through electrical stimulation, creating somatosensory percepts [16–18], and visual stimuli [19,20].

Longitudinal stability of recorded cortical neural activity has been investigated in both human and non-human primates, demonstrating that signals can be recorded from chronically implanted electrodes for up to four years [21–24]. However, longitudinal BCI performance from intracortical microelectrodes (such as the "Utah" array) varies widely between participants, as recording quality deteriorates over time [23,25–28]. Similar trends have been observed from Utah slanted electrode arrays during long-term peripheral nerve implants in human subjects [29] and animal models [30]. Biotic factors, such as inflammation and scar tissue encapsulation of the electrode sites, as well as abiotic degradation of device materials and mechanical failure from micro-movements of the electrodes relative to the brain, are all known potential degradation mechanisms for implanted microelectrodes [28,31–33].

Biological responses to implanted microelectrode arrays include glial activity and encapsulation of the implant in a glial sheath in response to the device being a foreign body [34,35]. These tissue responses can adversely affect the performance of the electrodes. For instance, a case study of a participant with a Utah array implanted for seven months revealed tissue damage correlated with decreased recording performance [36]. Implanted electrodes can also be displaced by meningeal tissue downgrowth, in some cases contributing to nearly 30% of chronic device failures in non-human primates [37–39]. Increased implantation durations have been associated with greater meningeal downgrowth, increasing distances from function neurons [40,41] and complicating the electrical pathways [38,42,43].

Material degradation presents another significant hurdle. Parylene-C, a common coating material for electrodes, can crack under physiological conditions [31,44–46]. Encapsulation damage has been associated with decreased electrode impedance in previous studies and can depend on the materials beneath the encapsulation coating [47]. All studies reporting longitudinal impedance of the Neuroport array have demonstrated substantial decreases in impedance asymptotically approaching values much lower than just after implantation [23,27]. Additionally, dissolution of silicon shank material in the harsh *in vivo* environment continues to be a critical issue for implanted silicon-based devices [45,47,48]. The mechanisms and kinetics for silicon degradation *in vivo* has not been fully determined and likely depend on multiple factors such as composition of the biological milieu, doping of the silicon, and fabrication processes.

The effects of electrical stimulation on electrode materials and surrounding tissues are crucial considerations for the long-term viability of BCIs. Aggressive electrical stimulation can erode sputtered iridium oxide films (SIROF) [49], another common coating material for electrodes, leading to a loss of functionality [50], though recent results suggest that SIROF optimization is improving the charge that can be delivered without degradation [51,52]. Mechanical failure of electrode tips (also observed on some control electrodes) is another common problem, potentially due to stimulation-induced degradation [53,54]

To evaluate the lifetime and performance of neural implants, several techniques have been utilized to quantify failure modes of chronically implanted electrodes. Measuring encapsulation of chronically implanted arrays (~1000 days for Pt and ~200 days for SIROF), researchers evaluated images procured with scanning electron microscopy (SEM) [55]. These preliminary results showed the prevalence of grossly damaged electrode tips correlated positively with duration of implant, in line with other pre-clinical studies [32,54]. Additionally, researchers noted irregular damage linked to stimulation, but did not describe a causal relationship. Accelerated aging techniques have been employed by Takmakov et al., using reactive oxygen species to simulate long-term degradation in vitro towards the establishment of known degradation mechanisms [56,57]. Additionally, a large number of animal studies have sought to correlatively link electrode performance with measurable degradation qualities such as impedance and known foreign body reactions and biochemical responses [31,58–61].

In short, the clinical viability of BCIs hinges on overcoming both biological and material challenges to provide a long-term stable interface for neural recording and stimulation. The objective of this study was therefore to assess potential damage to chronically-implanted intracortical microelectrodes and correlate the observed damage with measurable data collected throughout the implants' lifespans. This data may be informative for the design of next generation electrodes and further our understanding of electrode longevity and material design.

2. Methods

2.1. Terminology

Due to overlap of common terminology, we define some terms for the purposes of this paper. An *electrode* will be defined as a single shank on an array, comprised of a silicon shaft, insulation, and tip metal. An *electrode site* is the area with tip metallization exposed by removal of the Parylene-C insulation. *Shank* will refer to the silicon shaft within an electrode, which is 1.0 mm or 1.5 mm in length for FDA cleared arrays (K042384, K070272, K110010). An *array* will be the set of electrodes in a grid, typically either 10 × 10 or 6 × 10 (Fig. 1C,D,F,G). A *channel* will refer to data collected from a single electrode on an array. An *assembly* will be comprised of a Neuroport pedestal connected to one or multiple

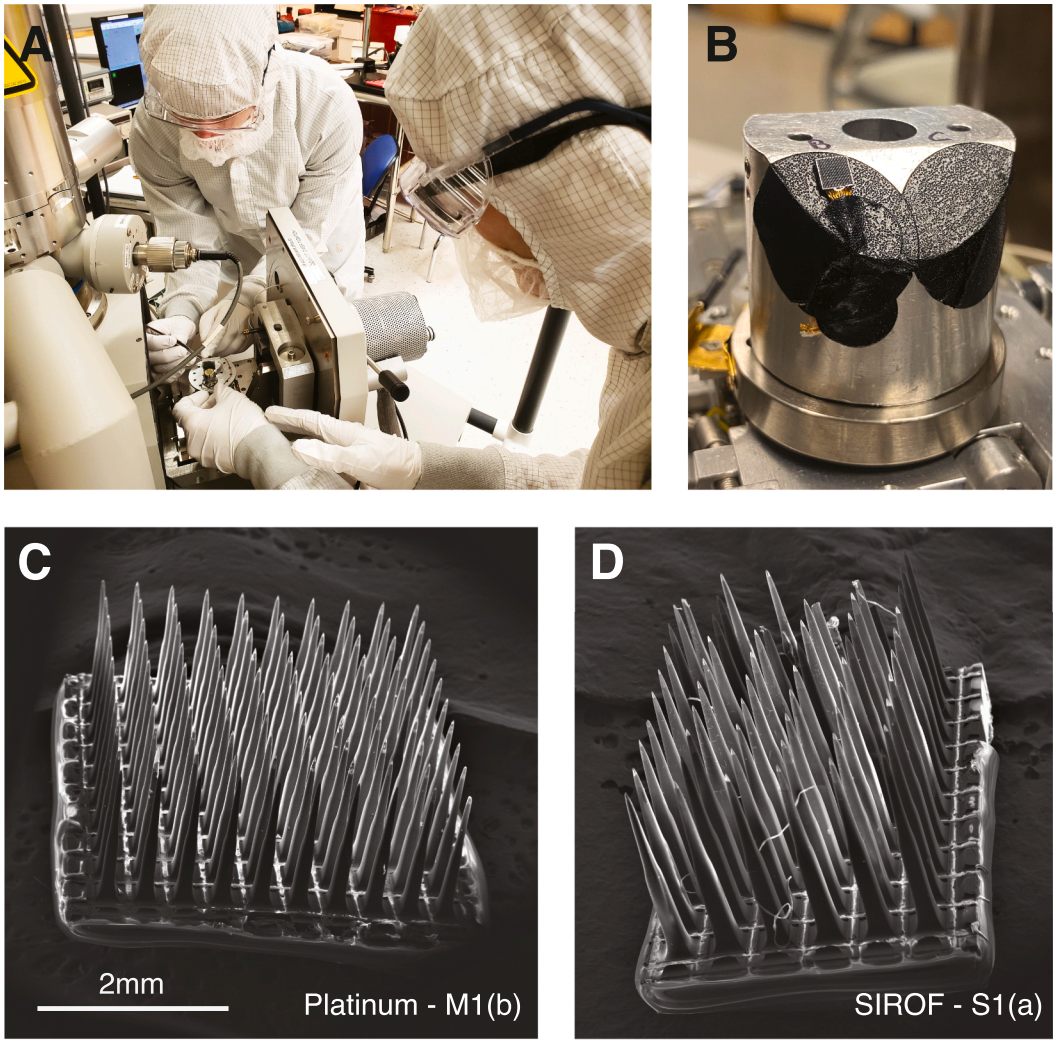

(caption on next page)

Fig. 1. SEM images of devices and implant locations. Scanning electron microscopy was used to captured the physical damage of each array. **(A)** Scanning electron microscopy images were obtained at the Kavli Nanoscience Institute at Caltech and University of Utah NanoFab. **(B)** Each electrode was fixed to the "chuck" with carbon tape and wire bundles grounded. **(C)** Whole array image of platinum tipped array (M1b) from the JHU/APL participant, explanted after 956 days. **(D)** Whole array image of sputtered iridium oxide film (SIROF) tipped array (S1a) from the JHU/APL participant, explanted after 956 days. **(E)** NeuroPort image from the manufacturer, Blackrock Neurotech, Inc. Not shown, but two reference wires were attached to the pedestal for implantation near the array. **(F)** Channel layout of connected and disconnected electrodes for each type of array, and location of the wire bundle. **(G)** Implant locations for ten implanted arrays. Participant from JHU was right handed, so contralateral referes to the *left* hemisphere. Both Caltech participants were only implanted in the *left* hemisphere. Full surgical implant details and procedures can be found at their respective publications.

arrays via a lead (wire bundle) of silicone encapsulated gold wires. Blackrock NeuroTech, Inc. (Salt Lake City, UT, USA) manufactured each of these arrays and assemblies. The company product documentation refers to an assembly of a single array and pedestal as a NeuroPort Array (Fig. 1E), and an assembly with multiple connected arrays to a single pedestal as a MultiPort Array.

2.2. Participants

Three human participants with C5-C6 level spinal cord injury were consented and chronically implanted with NeuroPort arrays [1,42,62]. All human subject research, experimental design and biomedical devices used for the participant in the Caltech/USC study were approved by the Institutional Review Boards (IRB) of the California Institute of Technology, University of Southern California, and Rancho Los Amigos National Rehabilitation Hospital for collection of this data in a registered clinical trial (NCT01849822). For the participant in the Caltech/UCLA study, all protocols were approved by Institutional Review Boards (IRB) of the California Institute of Technology and University of California Los Angeles (NCT01958086). For the JHU/APL participant, the study was conducted under an FDA Investigational Device Exemption; was approved by the FDA, the Johns Hopkins Institutional Review Board (JH IRB), and the NIWC Human Research Protection Officer; and is a registered clinical trial (NCT03161067). All participants gave their written informed consent prior to participation in research-related activities.

2.3. Devices

This work analyzed eleven microelectrode arrays as part of eight assemblies manufactured by Blackrock Neurotech for a total of 980 electrodes (Table 1). Ten of these arrays were chronically implanted in human cortex for 956–2130 days, and one non-implanted array served as a control sample. Two tip metal types were analyzed: platinum (Pt) and sputtered iridium oxide film (SIROF). Four Pt arrays had a 10 × 10 grid layout, with 96 electrodes connected to a single pedestal (Fig. 1F), and were implanted in human participants of the Caltech/USC [63] and Caltech/UCLA studies. Three *Multiport* assemblies were implanted in a human participant for the APL/JHU study, each comprised of one 10 × 10 Pt array (96 electrodes connected) and one 6 × 10 SIROF array (32 electrodes of the 60 connected) assembled to a single 128 channel Neuroport pedestal (Fig. 1F,G) [18]. During the explant surgery, each array was disconnected from the pedestal by cutting the lead. One Pt array (10 × 10) was manufactured at a similar time as the Caltech implantations and remained non-implanted and in the original sterile packaging for a duration of 1337 days between manufacturer validation date and SEM analysis. This array was imaged to serve as a control sample. These assemblies are laborious and time intensive to build, so the manufacturer validation date was used as the date of construction completion.

2.4. Implantation

The participant at Caltech/USC had one Pt array in *left* anterior intraparietal area (AIP) and one Pt array in left Brodmann's area 5 (BA5), which remained implanted for 2130 days (5 years, 10 months). The participant at Caltech/UCLA had one Pt array in *left* AIP and one Pt array in *left* Brodmann's area 5 (BA5), which remained implanted for 1988 days (5 years, 5 months). One human participant was implanted at Johns Hopkins with three Multiport NeuroPort assemblies (one Pt array and one SIROF array each attached to a single pedestal) for a duration of 956 days (2 years, 7 months). The right-handed participant had two Pt and two SIROF arrays in *left* primary motor and somatosensory cortex, respectively (contralateral M1 and S1), and one Pt and one SIROF array in *right* M1 and S1 (ipsilateral), respectively. Full details of surgical methods and array locations (Fig. 1G) can be found in prior articles for the first [63] and second Caltech participants [64], as well as the JHU/APL participant [18].

2.5. Explant procedure

Teams at Caltech/USC, Caltech/UCLA and JHU/APL explanted the three groups of arrays. The precise handling of the explanted devices could not be determined in all circumstances, but either involved rinsing in water and storage, or sterilization with an enzymatic cleaner, rinsing and storage. If sterilized, explanted devices were soaked in Enzol™ (Advanced Sterilization Products, Irvine, CA, USA), an enzymatic detergent used to sterilize medical instruments. They were then rinsed thoroughly in pure water, air dried, and stored dry in closed containers. Prior work has carefully evaluated the effects of Enzol on the composition and chemistry of Utah arrays and Parylene films and observed no changes [46]. Therefore, neither of the post-surgical handling procedures are anticipated to influence the results of this inspection. The lack of adhered soft tissue on the explanted devices suggests the enzymatic

Table 1
Timeline of electrodes.

Array Type	Size	Study Location/Participant		Implant Location	Shank Length	Validation Date	Implant Duration	Stim?	SEM Imaging
Pt	10 × 10	Caltech/UCLA	P1	AIP(a)	1.0 mm	6/9/14	2130 days	no	3/18/22
Pt	10 × 10	Caltech/UCLA	P1	BA5(a)	1.5 mm	6/9/14	2130 days	no	3/18/22
Pt	10 × 10	Caltech/USC	P3	AIP(b)	1.5 mm	10/15/12	1988 days	no	3/8/19
Pt	10 × 10	Caltech/USC	P3	BA5(b)	1.5 mm	10/15/12	1988 days	no	3/8/19
Pt	10 × 10	Caltech	-	-	1.5 mm	5/16/16	0 days (control sample)	no	1/13/20
Pt	10 × 10	JHU/APL	J1	M1(a)	1.5 mm	10/31/17	956 days	no	3/18/22
Pt	10 × 10	JHU/APL	J1	M1(b)	1.5 mm	10/31/17	956 days	no	3/18/22
Pt	10 × 10	JHU/APL	J1	M1(c)	1.5 mm	10/31/17	956 days	no	3/18/22
SIROF	6 × 10	JHU/APL	J1	S1(a)	1.5 mm	10/31/17	956 days	yes	3/18/22
SIROF	6 × 10	JHU/APL	J1	S1(b)	1.5 mm	10/31/17	956 days	yes	3/18/22
SIROF	6 × 10	JHU/APL	J1	S1(c)	1.5 mm	10/31/17	956 days	yes	3/18/22

cleaning procedure is more likely for all arrays.

During the explant of the Caltech/USC participant (Fig. 1: arrays AIP (a) and BA5), surgeons used a micro dissector to separate the wires from the cortex and arachnoid. They lifted each array circumferentially to extract each from the cortex. During the explant for the Caltech/UCLA study, both arrays were observed to be encapsulated with soft tissue. Removal of the devices left a clear impression in the tissue underneath, a common finding across all array locations (Figure S5).

Surgeons who performed the explant of the JHU/APL participant reported the skin was tightly adhered around the base of each pedestal, and indicated healthy skin tissue with no sign of infection. Arrays in the contralateral craniotomy (M1a,b, S1a,b) were extracted easily, with slight adherence to the cortical tissue. S1c was not removed intact, but M1c was extractable intact. Underlying cortical tissue appeared healthy with some fibrous tissue (Fig. S5). Most electrode arrays had some scar encapsulation.

2.6. SEM characterization

Scanning electron microscopy images were obtained at the Kavli Nanoscience Institute at Caltech (FEI Quanta 200, Thermofisher, Hillsborogh, MI) and University of Utah NanoFab (FEI Quanta 600, Thermofisher, Hillsborogh, MI) (Fig. 1A, Figure S4). Each of the 980 electrodes was imaged at 500x, 1200x, and 2500x magnification with simultaneous acquisition of backscattered and secondary electron signals, resulting in nearly 6000 images. The images were primarily collected using a 20 kV primary beam energy in high-vacuum conditions using solid-state detectors on the pole-piece for backscattered and Everhardt-Thornley detectors for secondary images. Working distances of 10 to 20 mm were used to enable imaging of both the whole array at low magnification, and the individual electrodes at higher magnifications. Backscattered imaging provides significant Z (atomic number) contrast, strongly facilitating discrimination between tip materials (e.g. silicon ($Z = 14$), Pt ($Z = 78$) and IrOx (iridium $Z = 77$, oxygen $Z = 8$)), and all other materials (e.g. Parylene-C or silicone backside and lead encapsulation). All images were collected without coating to improve surface conduction in order to maintain backscattered imaging contrast and to avoid alteration of the surface morphology. Occasional low-vacuum conditions were with the Large Field Detector (LFD) for secondary imaging when persistent charging disrupted imaging. Each electrode was fixed to the "chuck" with carbon tape and wire bundles grounded to the best possible extent with carbon tape over the wire-bundle and its cut-free end (Fig. 1B).

2.7. Longitudinal neural data collection

Throughout the lifetime of each implanted and connected electrode, impedance data and broadband electrophysiological waveforms were recorded at regular intervals using the Blackrock Cerebus Neural Signal Processor (NSP) to assess the electrode functionality and performance (Fig. 8). Electrodes at the four corners of all 10 × 10 Pt arrays were connected to patient ground, and 28 of 60 on the SIROF arrays were not electrically connected (Fig. 1F,G). Thus, no electrophysiological data were recorded from these electrodes, but they were imaged by SEM.

The magnitude of impedance was measured using the impedance measurement function of the Blackrock Cerebus and patient cable. Measurements used a 1 kHz sine wave with a magnitude of 10 nA peak-to-peak for 1 second, and the resulting voltage at electrodes recorded. The system cannot measure impedances <30 kΩ, and accuracy in the lower range of impedances deteriorates. This can impact the ability to accurately measure low impedance SIROF electrodes, particularly after long in-dwelling periods during which the impedances notably decrease.

Broadband electrophysiological waveforms were digitized at a 30 kHz sampling rate and hardware bandpass filtered between 0.3 Hz - 15 kHz. A software bandpass filter (250 Hz - 5 kHz) were applied to broadband signals to assess each electrodes' ability to record individual action potentials from surrounding neurons. Baseline noise was longitudinally measured through the life of the implant as the estimated root-mean-square (RMS) of the software filtered signal (Fig. 8D) [65,66]. The NSP analog headstages collected data from participants P1 and P3, while digital headstages collected data from J1. According the manufacturer's documentation, the input impedance of the NSP system (analog headstages) was 10^{12} Ω || 3 pF with an input referred noise of <3.0 μV rms (14 μV pk-pk). The NSP system (digital headstages) had input referred noise of 2.0 μV rms with an input impedance of 10^{9} Ω at 10 Hz and 10^{8} Ω at 1kHz.

2.8. End-of-study metrics for electrode functionality

Six experts systematically observed electron micrographs of the electrodes regarding five metrics of damage, scored as 1, 2, 3 or 4, from no damage (1) to severe damage (4) (Table 2, Fig. 2A). Scores from all experts were averaged for each metric. *Metallization* quantified the loss of metal at the electrode tip (Figure S3). *Separation* assessed the amount of separation between the silicon shank and tip metal. Nominally, the metal should be in direct contact with the silicon shank as part of the device fabrication. *Insulation* assessed thinning, penetration, and/or cracking of the *poly(chloro-p-xylylene)* (Parylene-C) along the outside of the shank. Parylene-C is expected to be a smooth and conformal layer in the region imaged near the electrode site. *Shaft* assessed damage to the silicone shaft. *Growth* assessed tissue adherence or bio-material damage to the electrode.

End-of-study impedance and neural data were measured and quantified prior to device explanation (Fig. 3). For each electrode array implanted at Caltech, six datasets of broadband recorded electrical activity were collected in the two weeks prior to explant, with the same parameters as those collected longitudinally. Three datasets were collected during the two months prior to explant for the JHU/APL arrays. Impedances were collected alongside each of these datasets for all electrodes (Fig. 3A). The recordings were used to determine noise and signal-to-noise ratio (SNR).

Single and multi-unit neural action potentials were identified by extracting waveforms which negatively crossed a threshold of −3.5 times the RMS noise (Figs. 3B, 8A). From the average waveform of the largest single neuron identified on each electrode, the SNR values were calculated as the ratio of waveform's mean peak-to-peak amplitude to its variance (Figs. 3C, 8A).

Stimulation efficacy was evaluated by quantifying the number of evoked somatosensory percepts via electrical stimulation patterns delivered through each of the connected SIROF electrodes. Using data collected during the last six months prior to explant, irrespective of stimulation pattern or frequency of use, each electrode was categorized as follows. Firstly, if a sensation was able to be evoked up to the end of

Table 2
Metric criterion for observed degradation.

Metric Name	Score Range	Criterion for Intact (1)	Criterion for Degradation (4)
Metallization	1 (intact) to 4 (severe degradation)	<10 % tip metal loss	greater than 90 % tip metal loss
Separation	1 (intact) to 4 (severe degradation)	no visible separation	any observed separation greater than 2 μm
Insulation	1 (intact) to 4 (severe degradation)	no observable deformations or all smaller than 5 μm	any observed deformations greater than 15 μm
Shaft	1 (intact) to 4 (severe degradation)	tip was wholly intact	>12 μm was fractured and/or missing
Growth	1 (intact) to 4 (severe degradation)	no adhesions observed or all adhesions smaller than 5 μm	any adhesion greater than 20μm

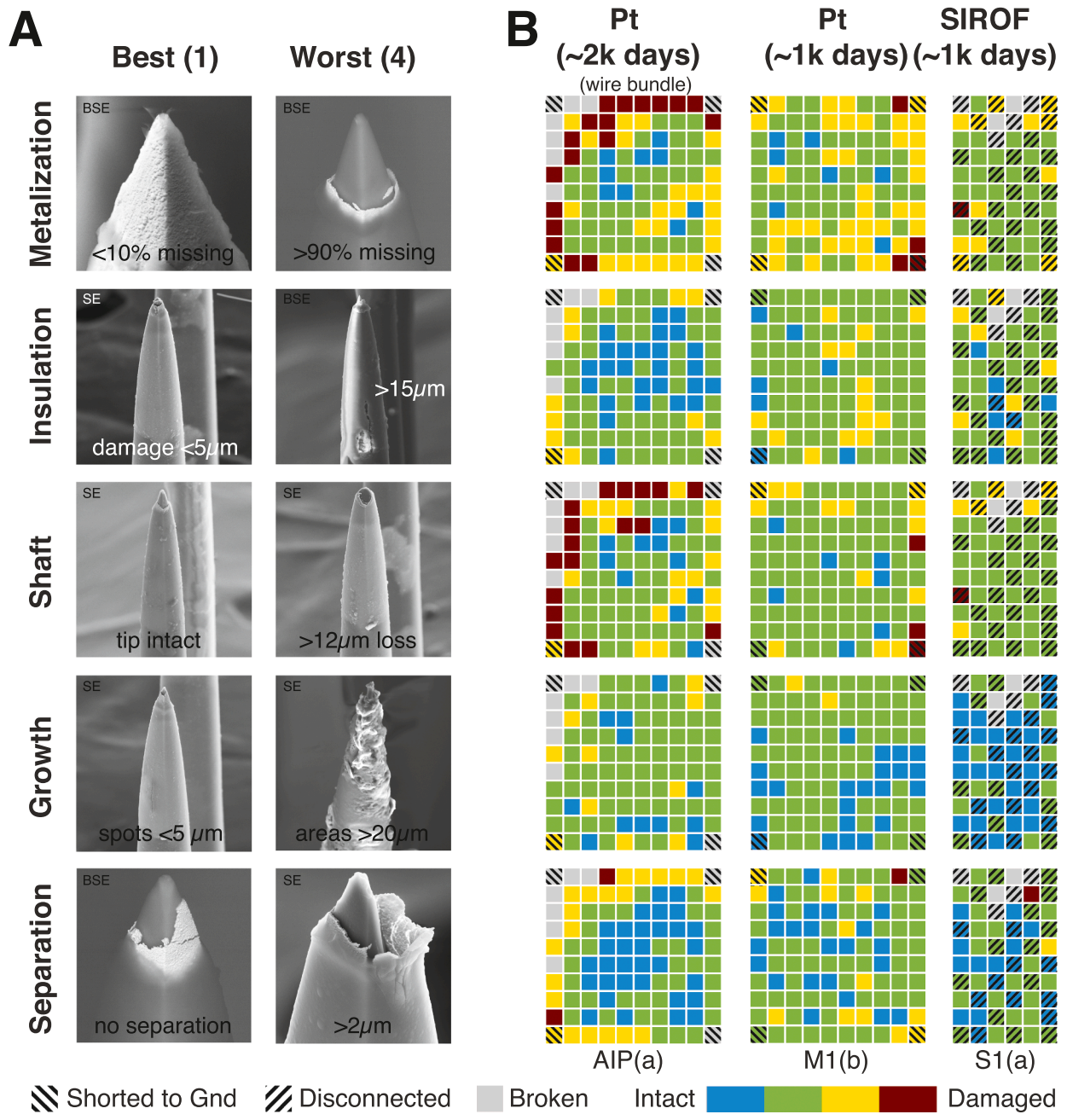

Fig. 2. Electron microscopy to categorize electrode condition (end of study). Scanning electron microscope imagery was captured of each electrode at three magnifications (500x, 1250x, 2500x) with a standard image (SE) and backscatter (BSE). Backscatter images highlighted metallization of the electrode tips while standard images captured topography from all material. **(A)** Humans scored each electrode by visual inspection of the images on a scale from 1 (intact) to 4 (damaged) on five metrics: metallization, insulation, shaft, growth, and separation. **(B)** Example heatmaps scored by one reviewer for each damage metric; blue refers generally to an intact electrode, while red indicates damage. Disconnected electrodes are marked with diagonal lines. Shanks which were completely broken off were excluded from the analysis (marked in grey). The heatmaps correspond to a platinum array at 1988 days (array AIP(a)), a platinum array at 956 days (M1(b)), and a SIROF array at 956 days (S1(a)).

study; secondly, if a sensation was previously evocable, but unable at end-of-study; and thirdly, if no sensation had ever been evoked (Figs. 3D, 8B). Total lifetime charge (milli-Coulombs [mC]) delivered through each electrode was also quantified to evaluate if the amount of stimulation correlated with electrode damage. The range of ICMS parameters were restricted by safety limits validated in NHP experiments [67]. Typical ICMS patterns were 0.5 – 1 s in duration, around 100 Hz pulse frequency and varied in amplitude from 5 to 100μA. Further information about ICMS tasks, parameters and patterns can be found in corresponding work [68–70].

The electrodes could have been damaged during several different intervals during their lifetime. One potential point of damage could have occurred during surgical handling and insertion into tissue. Additionally, abiotic (device) degradation or mechanical failure during chronic in-dwelling could also contribute to changes in performance metrics. Thirdly, explant or post-explant handing could have fractured or damaged the electrodes. By quantifying impedance, SNR, and stimulation efficacy (stimulation arrays) recorded just prior to explant (Fig. 3), we estimated the number of connected electrodes broken during the explant and/or transport phase (14/672 Pt) and (12/96 SIROF). Additionally, electrodes which were visibly destroyed (>50 % of the shaft gone) were removed from the physical degradation analysis (48/980 Pt

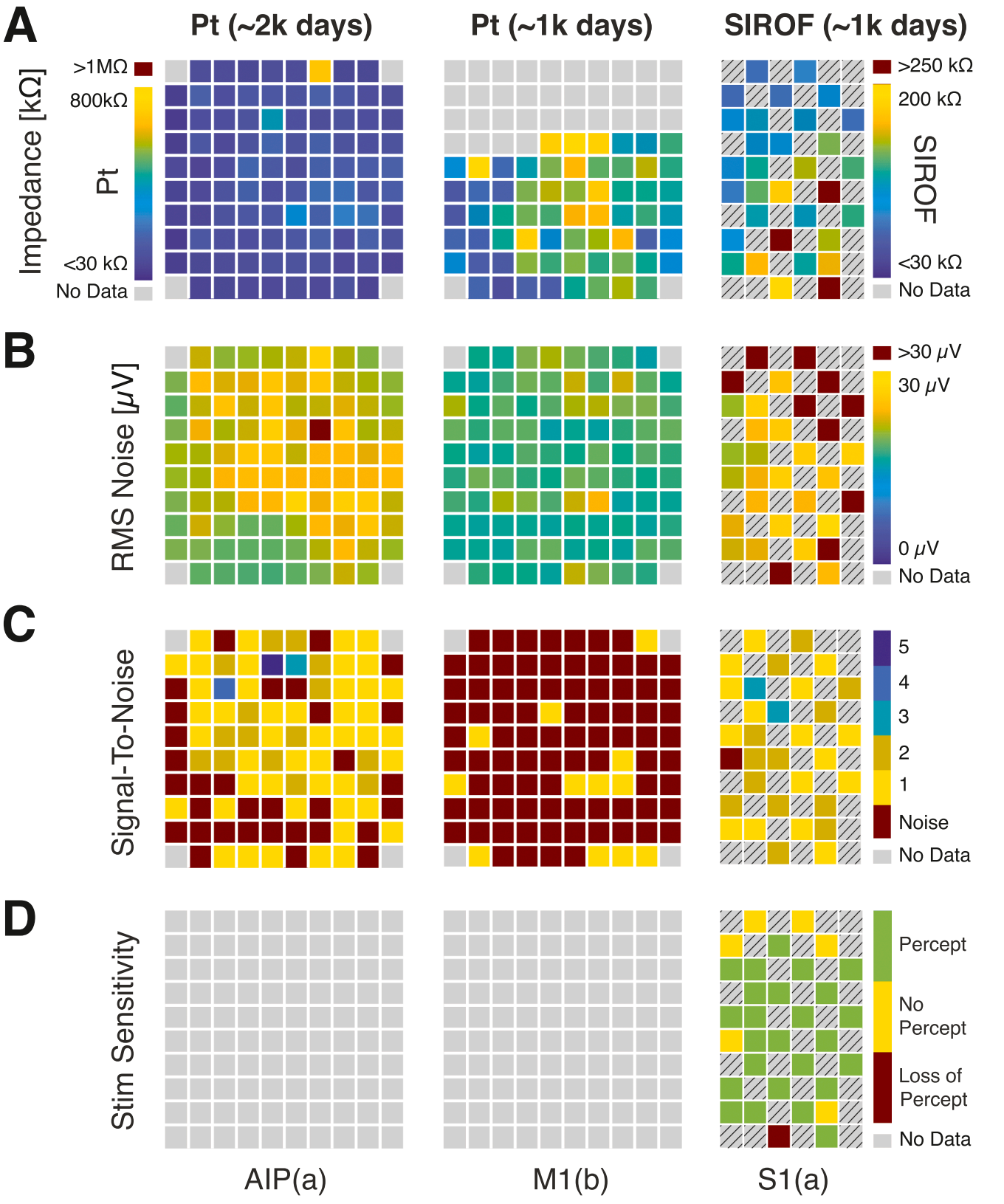

Fig. 3. Functional assessment of electrode quality (at end of study). Prior to explant, several measurements were collected to assess functionality of each electrode's condition: impedance, RMS noise, and signal-to-noise ratio. These data are presented from the electrode array AIP(a), M1(b), and S1(a), as identified in Fig. 1. Disconnected electrodes are marked with diagonal lines and grey boxes are for electrode shanks with no data. **(A)** Example heatmaps of a Pt array at +5 years of implantation. Impedance is shown from 200 - 800 kΩ for the platinum arrays (AIP(a) and M1(b)) and from 30 - 250 kΩ for the SIROF array (S1(a)). **(B)** Example heatmaps of RMS noise for the example arrays. We plotted RMS noise from 0 - 30 μV. Greater than 30μV was shown in red. **(C)** Signal-to-noise ratio as a heatmap for the example arrays. SNR ranged from 0 – 5. **(D)** We characterized each electrode as "able to generate a percept," "never generated a percept," or "generated a percept in the past, but unable to at end-of-study." Platinum and disconnected electrodes were never stimulated.

and SIROF). Thus, this assessment of electrode damage focused on underlying abiotic mechanisms during the in-dwelling period, not surgical placement and removal techniques. Biotic degradation mechanisms such as glial scar formation could not be analyzed, as this tissue was left intact during the explant procedure to minimize risks to study participants.

2.9. Statistical analysis

We used Spearman's correlation (with False Discovery Rate (FDR) correction for multiple comparisons) to test for significance in Figs. 6 and 7. *Moran's I* is a method of spatial autocorrelation [71], used to determine if damage indices are randomly arranged. Complete spatial randomness (CSR) is the null hypothesis ($I = 0$)) of a dispersed ($I = -1$) or correlated ($I = +1$) spatial structure (Fig. 6A). This represents the first time this spatial statistical technique has been applied to quantify the distribution of degradation of microelectrode arrays. For the violin plots in Fig. 4, we used a non-parametric, two-tailed-sample bootstrapped comparison of overlapping confidence intervals to assess significance.

2.10. Electrode groups

The 980 electrodes were grouped into five categories, excluding electrodes damaged during explant or transport phase: platinum after ~2000 days of implantation ($n = 389/400$), platinum after ~1000 days ($n = 293/300$), stimulated SIROF ($n = 84/96$), non-stimulated SIROF ($n = 72/84$), and control platinum imaged 1342 days after manufacturer validation ($n = 100$).

3. Results

This dataset of eleven arrays provided a unique opportunity to compare degradation characteristics across several different metrics (implant duration, electrode tip material, electrical stimulation, and electrical connectivity), while chronically implanted in human cortex. For each array, we quantified the severity of observed damage of each metric for each electrode, scored by experts, and correlated it to recorded electrophysiological signals and behavioral data collected at the end of the study (Fig. 4). Electrodes from the control array (not implanted) showed few signs of damage for any of the degradation metrics (Fig. 5, purple).

3.1. Implant duration

We observed an increase in damage correlated with implant duration (Fig. 5A), through a comparison of three groups of platinum electrodes (0 days: control, ~1000 days, ~2000 days). As expected, a majority of the degradation metrics (metallization, insulation, separation, growth; Figure S1) showed a positive correlation. However, we also observed a significantly higher amount of shaft damage in the implanted Pt electrodes at ~1000 days compared to ~2000 days (Fig. 4A – Shaft). The array M1(c) was observed to have notably higher levels of *shaft* damage serving as one mechanism for the differences. Small variations in shank thickness, likely due to variations in manufacturing, were observed in SEM images which is one possible cause for differences in shaft metrics.

3.2. Platinum vs. SIROF

At the time of explant, SIROF electrodes were nearly twice as likely to record neural activity as Platinum electrodes (Fig. 8, SNR), while implanted in the same participant for the same duration (965 days). For SIROF electrodes (Fig. 4, SNR: S1(a,b,c)), 67/96 had an SNR > 1 vs. only 97/288 for Pt electrodes (Fig. 4, SNR: M1(a,b,c)). Remarkably, we observed stimulated and non-stimulated SIROF electrodes had significantly higher damage than their Pt counterparts (Fig. 5B, $p < 0.05$, non-parametric, bootstrapped confidence intervals). Due to the heterogeneous distributions, these significance tests did not rely on an assumed distribution, however the mode/mean values did not always accurately represent the data (Fig. 5D).

We observed SIROF electrodes had significantly more tip metal damage than Pt electrodes. However, there was no significant difference between metallization damage on stimulated SIROF electrodes compared to their disconnected counterparts (Fig. 5C, Figure S2A). This may suggest stimulation was not the culprit for this increased metallization degradation between SIROF and Pt. In an additional analysis, we determined the amount of charge delivered also did not correlate with increased damage for any of our degradation metrics (Fig. 7B, $p > 0.05$, Spearman's rho). Damage to insulation and shaft were significantly higher ($p < 0.05$) for the SIROF electrodes (Figure S2A – Shaft, Insulation); however, tissue growth was significantly higher for the Pt electrodes. Additionally, Pt electrodes were more likely to have separation between the tip metal and shaft.

3.3. Participant-specific effects

We also observed variability in the degradation metrics within participants for the same type of electrodes on different arrays (Fig. 4, Metric: Metallization, Arrays: M1a, M1b vs. M1c). While the metallization, separation, and shaft damage for two of the Pt arrays (JHU/APL: M1a, M1b) were expectedly lower than the longer implanted electrodes (Figure S1B,C vs. S1D), the array implanted in the *right* (ipsilateral) hemisphere (JHU/APL: M1c) was a clear outlier in damage, despite being the same electrode type (Pt) and having the same implantation duration (956 days) as M1a and M1b.

We also observed significant differences between platinum electrodes implanted for similar durations in different participants (Figure S1B,C). Metallization and separation damage were clearly higher for the arrays in the second Caltech participant (Figure S1C) than the first (Figure S1B).

3.4. Stimulated vs. disconnected electrodes (SIROF)

Investigating the effects of stimulation in human cortex and the longevity of such electrodes was a key aim of this study. Of 60 electrodes on each SIROF array, there were 28 electrodes not electrically connected (floating) (Fig. 1G). These electrodes provided a good control for potential damage caused solely by electrical connection, stimulation, or their combination. Due to the checkerboard pattern of connected and disconnected electrodes on the SIROF arrays (Fig. 1G), stimulated and disconnected electrodes were evenly spatially organized.

Across the damage metrics from SEM inspection, we did not observe many significant changes in the degradation between stimulated and non-stimulated electrodes (Fig. 5C, Figure S2). Slight but significant increases in insulation damage occurred, as well as an increase in observed growth on the stimulated electrodes.

3.5. Type of damage correlated with stimulation

While inspection of the electrodes did not show significant differences in the *amount* of metallization damage between stimulated and disconnected electrodes (Fig. 5C), we did identify significant differences in the *type* of damage (Fig. 6B, Cracked vs. Pockmarked). The vast majority of the metallization damage observed on the platinum electrodes (Fig. 6A) could be described as a "cracking" or "flaking" of the metal, peeling away from the silicon shaft (Fig. 6D).

We observed a different type of damage to the metallization, which we have named "pockmarked," primarily occurring on the stimulated SIROF electrodes. This damage could also be described as "beading," "melting," or "congealing" of the tip metal. It is reminiscent of thermal damage, but there is not a commonly reported mechanism for such damage to occur within the *in vivo* conditions that divides these two populations. No significant temperature changes occurred for this metal

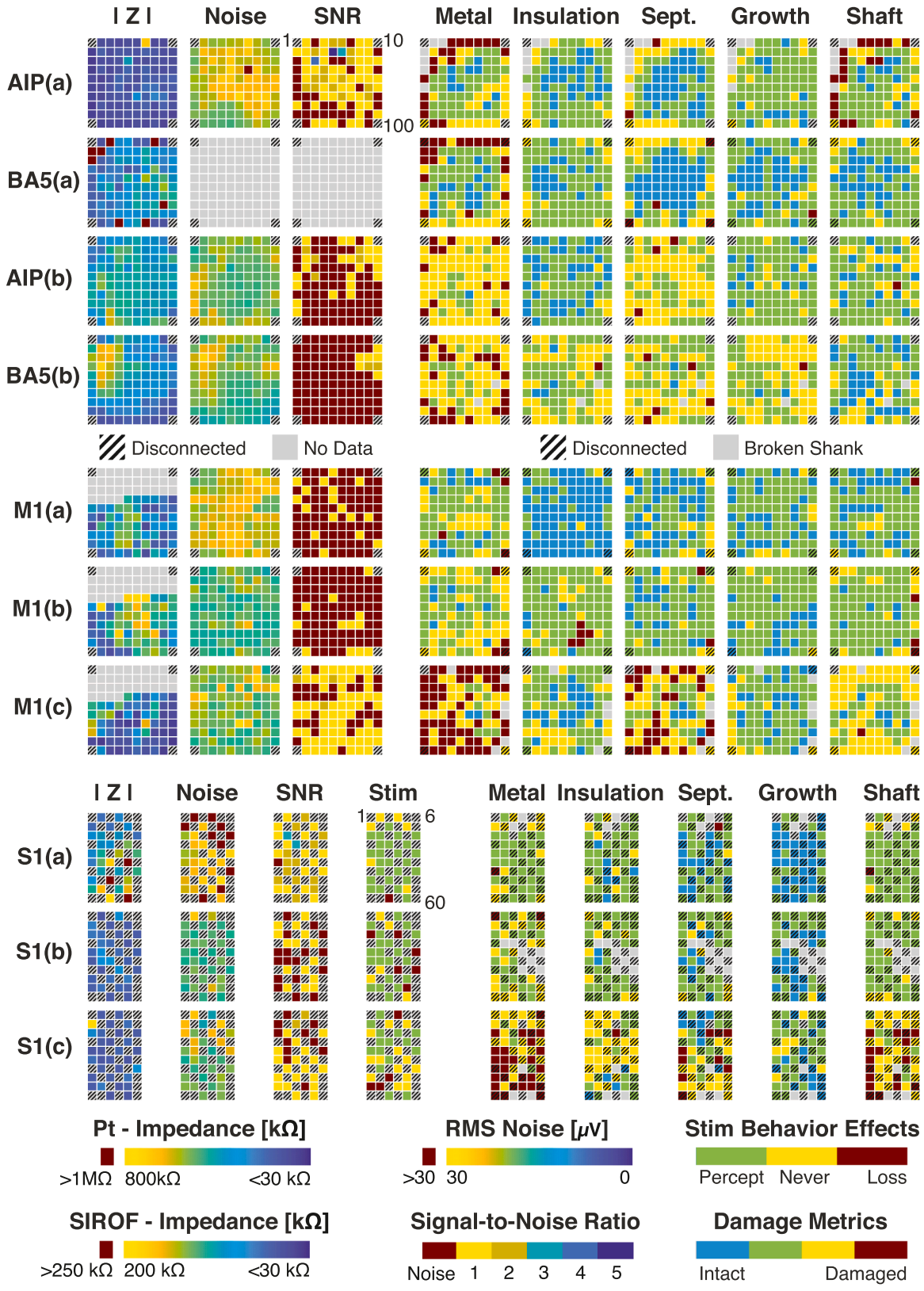

Fig. 4. Heatmap of all electrodes and metrics (at end-of-study). Complete spatial maps for all arrays analyzed. Channel numbering starts from the top left corner, proceeding left to right, top to bottom. The wire bundle was connected to each array from the top of this layout. Scale bars indicating range of [kΩ] for impedance, μV for RMS noise, as well as average damage metrics, visual assessed from SEM images by experts. For all scale bars, blue refers generally to an intact electrode, while red indicates damage. Grey boxes have no data for Impedance (|Z|), RMS Noise, SNR, and Stim. Broken shanks are indicated with grey boxes for the visually-assessed damage metrics.

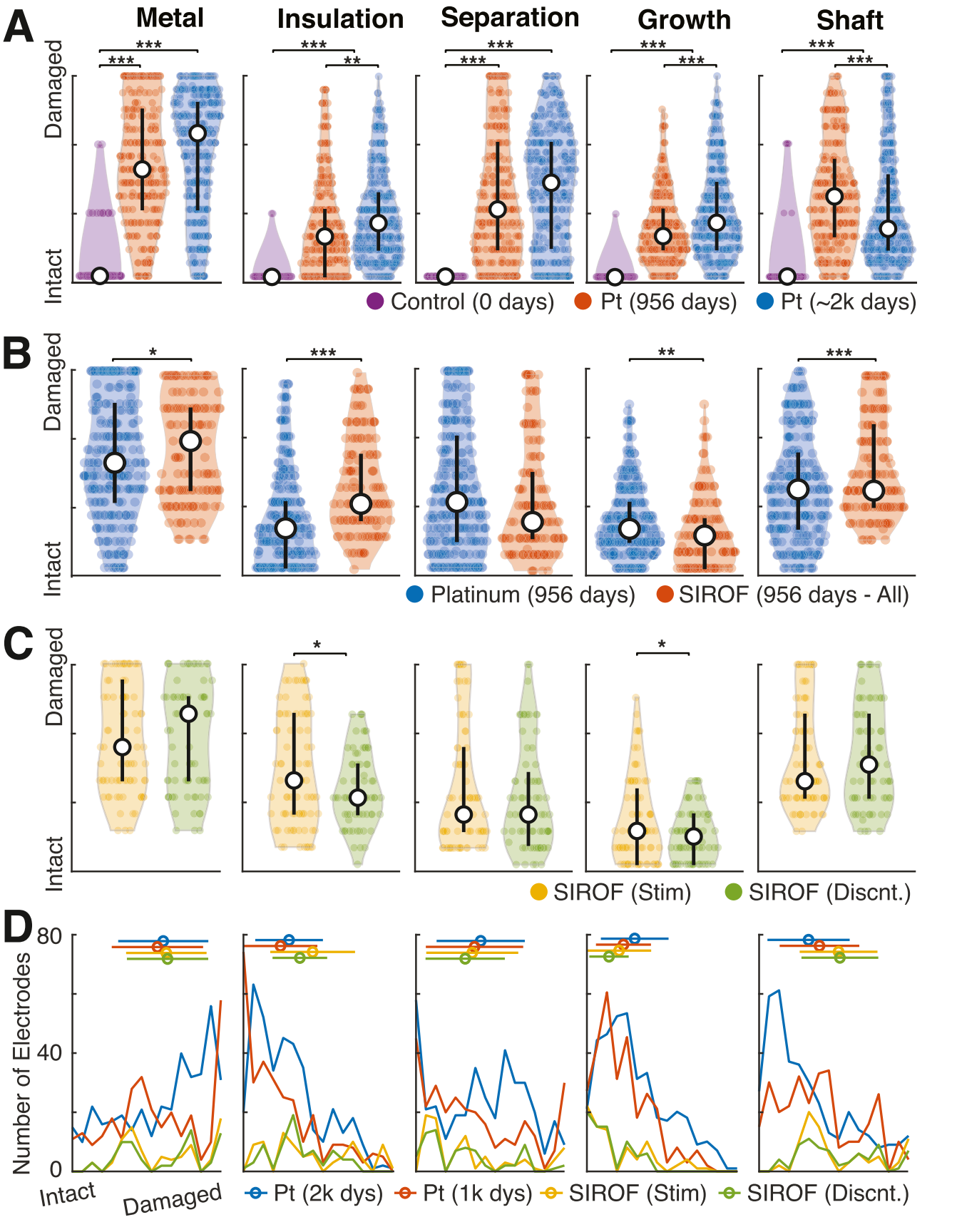

(caption on next page)

Fig. 5. Degradation characteristics. Electrode scores for each metric visually scored by human experts were grouped according to implant duration (0 days: control, ~1000 days, ~2000 days), stimulation vs. disconnected, or tip material (Platinum vs. SIROF). Plots show the distribution of scores (violin plot), median score (white circle) and quartiles (black line). Significance was assessed via non-parametric two-sample bootstrapped confidence interval comparison and is indicated by black bars. Additional displays of array-specific information is provided in Figure S1. **(A)** Degradation on the platinum electrodes over time was observed for most metrics. Shaft damage was more prevalent on electrodes implanted for only ~1000 days (JHU/APL participant) than those implanted for ~2000 days (Caltech participants). **(B)** We observed significantly higher rates of damage to the metallization, insulation, and shaft on the SIROF shanks than then Pt shanks. Shaft damage was highest on the shanks implanted in the JHU/APL participant (all electrodes 956 days). **(C)** For SIROF electrodes implanted in the same participant for the same duration (2.6 yrs), we compared observed damage on electrodes through which stimulation was delivered and disconnected electrodes (see Fig. 1G for spatial organization of SIROF electrodes). Two of the five damage metrics (insulation and growth) were statistically significantly worse for electrodes that had delivered stimulation vs. those that were discontinued. **(D)** Detailed histogram comparing all groups of electrodes. Mean and standard deviation are illustrated as a line and circle above the histogram. Further breakdown by array can be found in Fig. S1 and S2.

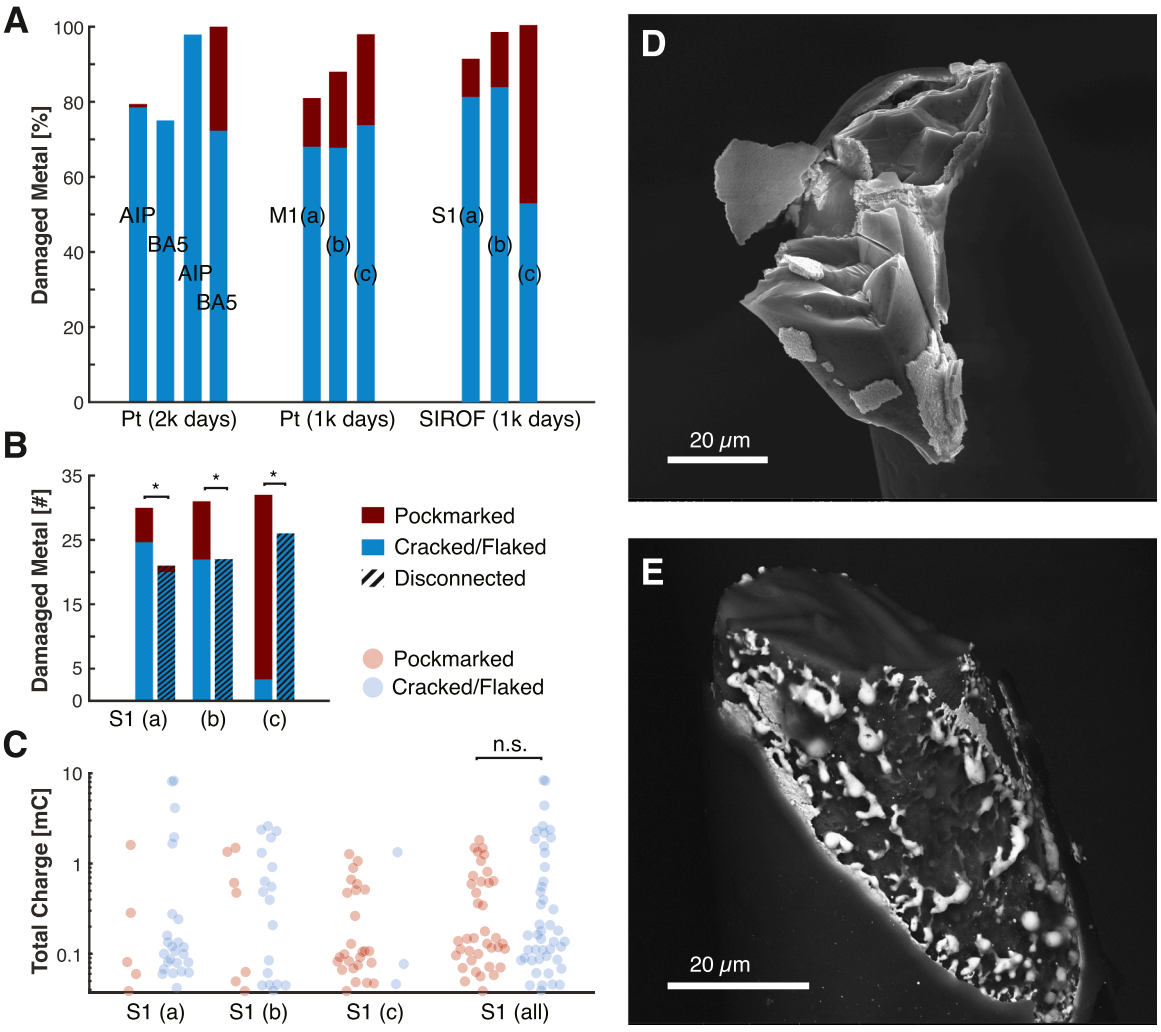

Fig. 6. Tip metal damage. We observed and quantified two types of tip metal degradation: Cracking/Flaking (depicted in blue in the graphs) and Pockmarked (in red). **(A)** Pockmarked electrode tips were present on most arrays, but most prevalent on SIROF tips. Most arrays had >80 % of electrodes with some metal damage. **(B)** When comparing electrodes which were stimulated to those which were disconnected, we can observe stimulation-specific effects. Pockmark degradation features were significantly more present on stimulation electrodes vs. disconnected ones. Stimulation electrodes were also more likely to have metal damage than the disconnected ones. **(C)** The total charge delivered through each damaged electrode in the SIROF arrays (S1(a), S1(b), S1(c), combined) is plotted in milliCoulombs (mC). The *type* of tip metal degradation was not correlated with the total amount of delivered charge. **(D)** SEM backscatter image of a SIROF electrode with cracked/flaking metal. See Fig. S3 for more examples. **(E)** SEM backscatter image of a SIROF electrode showing pockmarked metal degradation.

deformation. The potential across the electrochemical interface (E_{mc}) is not expected to have been sufficient to drive the metallurgical reactions that might result in deposition of metal, which is the mechanism by which rounded deposits of metal can form. Additionally, the damage resulted in exposure of the silicon shank under the metallization. It appears the SIROF material melted away and reattached itself to the silicon shaft in small nodules (Fig. 6E), which speculatively could result from local gradients in the potential across the surface.

This observed "pockmarked" damage occurred with significantly higher frequency on stimulation electrodes vs. disconnected ones (Fig. 6B), suggesting that stimulation may accelerate or enhance this form of metallization damage rather than the more typical "cracking" or "flaking." However, it was also present in limited amounts on the platinum electrodes, thus stimulation is not the only way for this degradation mechanism to occur (Fig. 6A). We also compared the amount of delivered charge through each stimulation electrode and did not see a

significant between the metallization degradation types (Fig. 6C), adding evidence that low current stimulation did not exacerbate damage beyond that caused by chronic implantation in human cortex.

3.6. Spatially correlated damage

Most of the assessed damaged metrics were significantly spatially correlated (Fig. 7A). Using Moran's *I*, a measure of spatial autocorrelation (−1 indicates a fully dispersed pattern, 1 indicates full spatial correlation), we observed significant spatial correlations between SEM-inspected damage metrics and end-of-study measurements of electrode performance. The *in vivo* milieu surrounding the electrodes is not expected to have large variations in composition across the surface of electrodes that could lead to the correlation and grouping of damage observed. Such gradients could exist due to more chemical access to edge electrodes, and due to decreased of vascular access to the interior electrodes of the array. Edge electrodes are more likely to be damaged during fabrication and handling, and such damage could contribute to degradation *in vivo*.

3.7. Significant correlations between all damage metrics

Observed physiological damage of the electrodes affected multiple damage metrics rather than just a single feature (Fig. 7C). For SIROF electrodes, the amount of growth on the electrode significantly correlated (rho > 0.5) with all other metrics, indicating a potential mechanistic driver for other degradation features. For both SIROF and Pt electrodes, metallization and separation had the highest correlation (rho > 0.75).

3.8. Impedance correlates with SIROF electrode recording and stimulation performance and degradation

A primary aim of this study was to link observed electrode degradation to electrode functionality: recording neural activity and delivering stimulation (for SIROF only). We computed the correlation between each end-of-study electrophysiological measurement and each of the damage metrics from SEM (Fig. 7B).

We found impedance to be highly correlated (Spearman's rho, FDR correction) with all damage metrics observed by SEM for SIROF electrodes, but not for Pt electrodes (Fig. 7B). This finding suggests impedance is a good measure of electrode damage for SIROF electrodes and should be continually measured throughout the implant lifetime to monitor electrode performance.

Impedance significantly correlated with recording performance for SIROF electrodes. Despite the higher noise of SIROF electrodes (Fig. 8A, Noise), they achieved superior single unit recording characteristics (Fig. 8A, Signal-to-Noise). Both noise and SNR significantly positively correlated with impedance measurements (Fig. 7D, Impedance).

Impedance also significantly correlated with SIROF electrode stimulation performance (Fig. 7D, Sensation). The functional ability of the SIROF electrodes to create a somatosensory percept (Fig. 8B) was significantly negatively correlated to several damage metrics (Fig. 7B), suggesting that increased electrode damage may decrease the likelihood of evoking a sensation. Importantly, we found that total charge delivered on stimulated SIROF electrodes did not significantly correlate any of the damage metrics (Fig. 7B).

In contrast to the SIROF electrodes, impedance and SNR were negatively correlated for platinum electrodes (Fig. 7D, Impedance); suggesting lower impedance Pt electrodes and higher impedance SIROF electrodes had the highest SNR values.

3.9. Longitudinal electrode performance

All electrodes demonstrate a decrease in impedance and noise with time, consistent with analysis from other groups [21]. Such decreases would typically be attributed to encapsulation degradation, which could be consistent with decreased noise due to more averaging over a larger surface area. This suggests the optimal impedance and noise characteristics for detecting signal units, depend on a complex interplay between electrode material, exposed area, and associated noise characteristics.

Importantly, there are trends between longitudinal impedance and noise (Fig. 8C,D). At early time points, the SIROF arrays have notably higher noise values and notably lower impedances. Most electrodes showed an initial high spike in impedance immediately post-implantation, with a gradual decay, reaching nominal ranges within the first year (200–800 kΩ for Pt, 80–200 kΩs for SIROF). RMS noise generally settled into nominal ranges (14–28 μV) after the first 100 days, with the exception of array S1(c). For the platinum arrays, this "settling" occurred much faster, generally within the first 25–50 days.

4. Discussion

A primary goal of this study was to quantify the condition and possible damage to chronically-implanted Neuroport electrodes and link observed damage to available, measurable data throughout the lifetime of the implant. We examined 980 electrodes implanted in three different BCI participants, comparing the effects of implant duration, electrode type, wired vs. unconnected, electrical stimulation, and the charge delivered by electrical stimulation. We imaged all electrodes using scanning electron microscopy and evaluated each for five components of damage, including metallization, insulation, shaft, growth and separation. We also captured end-of-study measurements just prior to explant: impedance, RMS noise, SNR, and stimulation functionality.

In general, we observed more severe damage on electrodes implanted for longer durations. Our data showed no correlation between electrode damage and the amount of delivered stimulation, but we did see a significant difference in the connected (wired) versus unconnected electrodes from the SIROF stimulation arrays. We also identified a new type of degradation feature (referred to as "pockmarked"), correlated with the prior delivery of stimulation, but also occurring on a few Pt electrodes. Impedance measurements were significantly correlated with 1) all five damage metrics observed by SEM for SIROF electrodes, 2) recording performance as measured by SNR, and 3) stimulation performance. Together, these data suggest impedance may be a valid performance measurement for these types of electrodes. Despite better recording performance at end-of-study (measured by higher SNR values), SIROF electrodes fared worse in damage compared to platinum electrodes; suggesting these electrodes may be better at capturing single neuron activity, despite damage.

4.1. Impedance strongly correlates with observed damage on SIROF electrodes but not Pt electrodes

In absence of any other defined metrics or observable variables, measuring electrode impedance has long been the gold standard in determining *in vivo* electrode performance [31,72–75]. However, as electro-physiologists commonly note, correlation between the 1 kHz impedance magnitude and signal performance is tenuous at best [76,77]. This study validates these fears with respect to platinum electrodes, for which impedance was weakly correlated with observed damage (Fig. 7B – Impedance: blue, green). However, impedances collected from SIROF electrodes strongly correlated with all observed damage metrics (Fig. 7B – Impedance: yellow).

From prior literature, the tip material and surface area exposed play a significant role in impedances changes [47]. We hypothesize physical damage to the tip material and surface area may have an outsized impact on impedance for SIROF, given the much lower range of impedances (Fig. 8A); however, further experimentation beyond the scope of this manuscript are required for confirmation.

As expected from previous studies, impedances for all arrays

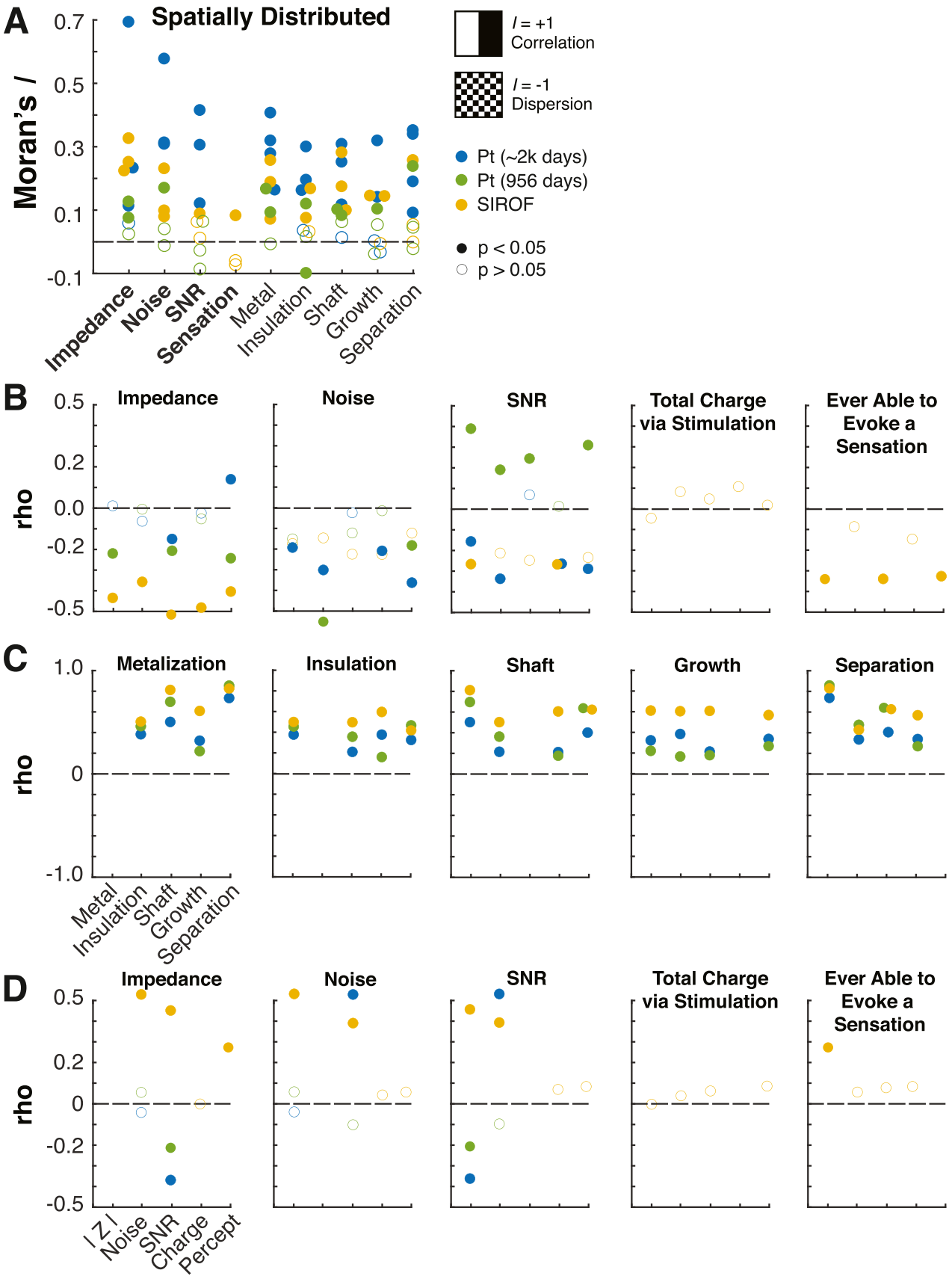

(caption on next page)

Fig. 7. Analysis of observed damage. We evaluated relationships between damage metrics (metallization, insulation, shaft, growth, separation) and end-of-study metrics (SNR, impedance, noise). Filled in circles indicate statistical significance ($p < 0.05$). **(A)** Using Moran's *I*, a measure of auto-spatial correlation, most metrics we observed were spatially correlated, suggesting damage was not due to implant/explant procedure but rather biological breakdown or tissue interaction. **(B)** We evaluated Spearman's rho correlation between damage metrics and end-of-study metrics. Impedance significantly correlated with all damage metrics for SIROF electrodes, but was weakly correlated on Pt electrodes. The total charge delivered via stimulation did not correlate significantly with any of the damage metrics. **(C)** All damage metrics were positively correlated together, suggesting that no one metric occurred in isolation. Metal and separation metrics had the highest correlation for all groups ($r > 0.75$), while growth was positively correlated for SIROF electrodes for all other groups. This suggests a possible mechanistic driver for degradation for these types of electrodes. **(D)** SIROF electrodes had a significantly positive correlation between: impedance and RMS noise, Impedance and SNR, and RMS noise and SNR. Pt electrodes explanted at 956 days had a significantly negative correlation between Impedance and SNR. Pt electrodes explanted at 2130 days had a significantly negative correlation between Impedance and SNR, and a significantly positive correlation between RMS Noise and SNR. The total charge delivered via stimulation did not correlate with any of the other end-of-study measurements. Platinum and SIROF were oppositely correlated between impedance and SNR. The optimal impedance that correlates with detecting single units lays somewhere in the upper range of the SIROF electrodes and in the lower range for platinum, in a process that could involve tip materials and deinsulation length.

generally decreased over time (Fig. 8C), likely due to a combination of encapsulation [28,77], metallization breakdown, and increased exposed electrode surface area. This longitudinal trend correlates with increased degradation over time [55].

4.2. Proposed degradation mechanisms

We observed a variety of electrode metallization failure modes and sought to characterize a potential timeline and mechanisms for such degradation (Figure S3). We observed a high frequency of electrodes with highly damaged tip metal (Figs. 3, Metallization); however, some electrodes remained in near perfect condition (Figure S3A). The electrodes ranked "Intact" (Figure S3A,B,C) exhibited no imperfections or slight damage, including the very top of the electrode and/or hairline fractures or holes in the metallization at the base of the tip (Figure S3C). While damage might be present below the metallization as has been observed previously [46], these results are suggestive that achieving improved stability for electrodes is possible. Whenever we observed the holes in the tip metal, we also observed etching of the silicon shank underneath, likely causing separation between the metal and the silicon (Fig. S3D-I). With severe etching/erosion, we observed flaking of the tip metal, often with such remnant flakes observed in the images (Figure S3G-I). At the worst case, we observed nearly all the metal had been mechanically removed due to undercutting (Fig. S3 J) and/or the silicon shank had been severely etched (Figure S3 K,L).

In several cases, there appears to be consistently oriented fracture surfaces in the silicon shank of multiple electrodes potentially leaving them more susceptible to etching, contributing to large parts of the electrodes peeling away. By careful evaluation of the fracture surfaces, one could estimate a a timeline for when such fractures occurred. Brittle fracture surfaces of exhibit mirror, mist, and hackle zones [78], with the latter having sharply defined features. Prior and current observations have shown silicon serves with smoothened features consistent with being etched *in vivo*. These features are often coincident with separations between the metallization and silicon, providing evidence that silicon dissolution contributes to smoothening features. Electrodes with both sharp and smoothened characteristics were observed, but quantifying such characteristics is beyond the scope of this work.

Some component of the observed variability of electrode longevity may be due to manufacturing differences (these would be an uncontrolled noise variable) [31]; however determination of this is beyond the scope of this dataset. Additionally, rigorous testing of our silicon corrosion hypothesis would require significant experimentation, best accomplished with bench studies such as electrochemical corrosion studies [79] to precisely identify the mechanisms at work. This could be followed by *in vivo* animal studies to verify degradation mechanisms or mitigation strategies similar to prior work with Utah arrays [46] and Michigan probes [48]. Factors such as the doping concentration, integrity of the tip metallization and encapsulation layers or potential other process factors might affect the longevity and performance of silicon based neural electrodes.

4.3. Relationship between recording performance and physical degradation

The signal-to-noise ratio (SNR) may be one of the most important BCI functional/performance metrics since the quality and quantity of neural activity will dictate the performance ceiling of any therapeutic device. We observed intuitive results for SIROF electrodes (Fig. 4, S2), SNR significantly correlated *negatively* with 2/5 damage metrics (Fig. 7B: SNR, yellow dots). As expected, lower metallization and growth damage correlated with higher SNR.

For platinum electrodes, we observed divergent results. For Pt (~2000 days), AIP(a) had higher SNR and lower metallization damage, while AIP(b) and BA5 showed lower SNR and lower damage (Fig. 4, S1). SNR significantly correlated *negatively* with 4/5 damage metrics (Fig. 7B: SNR, blue), just as SIROF electrodes performed. However, for Pt electrodes (~1000 days), M1(c) showed high SNR and high damage. And M1(a,b) showed comparatively lower SNR and low damage (Fig. 4, S1). For these Pt electrodes, SNR significantly correlated *positively* with 4/5 damage metrics (Fig. 7B: SNR, green).

These conflicting data highlight the variability present in the Platinum electrode population and consistency among the SIROF. Additionally, we see 0/5 degradation metrics significantly correlated with measured noise (Fig. 7B: Noise, yellow), suggesting the SIROF noise may be more resilient to physical damage than Platinum electrodes (where 4/5 metrics significantly correlated).

4.4. Highly damaged electrodes can still yield good neural recordings

Some electrodes observed to have "high damage" captured good quality neural signals during the end-of-study measurements (SNR > 1). An example electrode (Fig. 4– Array AIP(a), Channel #5), scored the worst rating on metallization and shaft damage, and the second-worst rating on separation damage. However, during the end-of- study measurements, this electrode had an SNR of 2, meaning a significantly large single-unit waveform was recorded while impedance measurements appeared nominal.

This finding was commonplace throughout our dataset. For the ~2000 day platinum electrodes, 150/389 were marked as "high damage" (at least one degradation metric score > 3.5). And of these "high damage" electrodes 45/150 had good quality signals (SNR > 1). For Pt (956d), we saw similar percentages: 94/293 "high damage" electrodes, of which 53/94 had good SNR. For connected SIROF electrodes, 36/96 had "high damage", while 24 of those had good SNR.

Two justifications may partially explain this incongruency. Firstly, physical characterization of electrical connectivity between metal and silicon may be difficult to accurately judge. SEM images obtained approximately 180–270° of coverage of the round electrodes, leaving a small blind spot on the back side of the electrode preventing observations of regions potentially conducive to recordings. A precise test of electrical functionality (i.e., impedance measurements post-implant) may more accurately capture such information; however, due to surgical requirements during explant, the wired connection between the

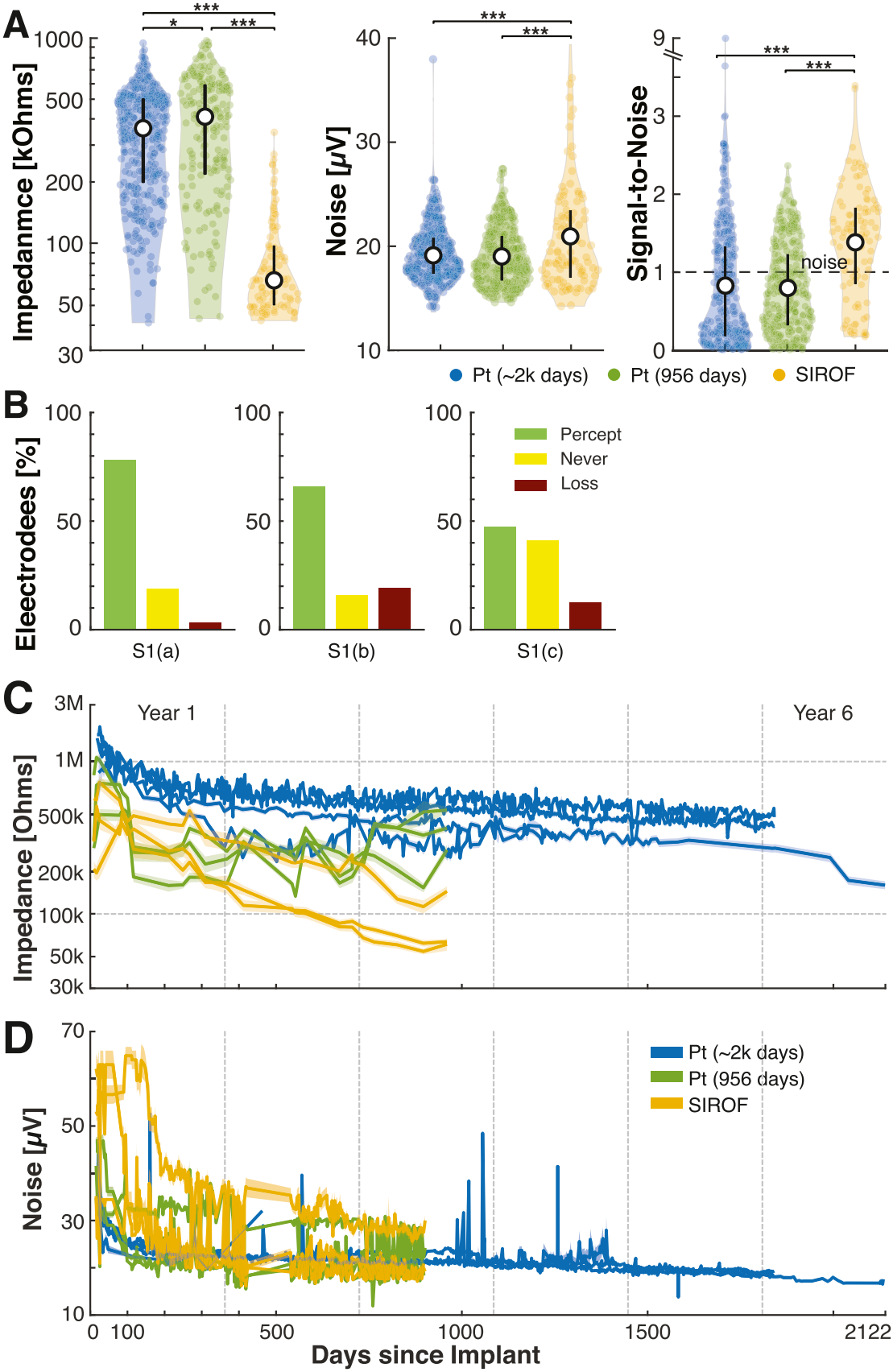

(caption on next page)

Fig. 8. Electrode functionality. Longitudinal measures of electrode health were collected throughout the duration of the implantation and directly prior to explant. **(A)** As expected, measured impedance was significantly higher for both groups of Pt electrodes than SIROF at end-of-study. RMS noise was significantly higher for SIROF as well as recording performance, measured by the signal-to-noise. SNR was measured as the ratio of the mean peak-to-peak waveform to its variance. **(B)** For each of the SIROF arrays, the majority of the electrode were able to evoke a sensation at some point during its lifespan (green + red). A small number of electrodes stopped evoking sensations prior to explant (red). The y-axis shows a histogram of the percentage of SIROF electrodes in each condition. **(C)** Impedances for all electrodes were initially higher than their specified ranges immediately after implant. They quickly settled into their respective operating ranges within the 100 days. **(D)** Noise was assessed via an RMS calculation and remained relatively stable after the first 200 days post-implant. Values generally decreased with time, with occasional large outliers. These outliers often corresponded to noise in the signal, degradation of filament in the analog cables or other sources of environmental noise. Shaded error bars refer to 1 standard error of the mean of all electrodes on given array.

pedestal and array is severed, making such measurements impossible. Secondly, small aspects of metal physically and electrically attached to the silicon shaft on undercut surfaces or other features may yield sufficient surface area to enable recordings. These results suggest only quite small electrode areas might be necessary to capture neural signals. In this best-case scenario, electrodes may be able to tolerate significant damage and yet remain viable for recording.

Whichever hypothesis future studies confirm, our observations do provide some reasoning behind the ability of electrodes to continue to function well into the realm of >1000 days of chronic implantation, despite known degradation [21–24].

4.5. Limited degradation on stimulating electrodes

Across three stimulation arrays and five degradation metrics observed from SEM imaging, we found partial evidence of additional damage caused by stimulation (Fig. 5, Fig. S2). Electrodes which were stimulated displayed significantly higher insulation damage and tissue growth adhered to the electrode. In contrast to previous findings from a much shorter time scale (182 days) [55], we did not observe an increase in metallization damage. Given the large changes in impedance and inflammation response during the first six months of implant, it is possible the electrode interface had not yet stabilized in the prior study [21].

While the frequency of metallization damage was not significantly different from stimulation vs. non-stimulation SIROF electrodes, our imaging has revealed a new type of electrode tip metal degradation, predominately observed on stimulating electrodes (Fig. 6B). This "pockmarked" degradation is markedly different in visual characteristics to traditionally observed metal degradation which often appears as "cracked/flaking" (Fig. 5D vs. 5E). This new "pockmarked" metallization damage was also observed on non-stimulated platinum and SIROF electrodes (Fig. 5A,B), albeit at a much lower frequency of occurrence. We hypothesize stimulation may accelerate this damage type but not be the sole cause, since it is not unique to stimulated electrodes.

Furthermore, the total charge delivered through a stimulating (SIROF) electrode did not significantly correlate with any of our visually-assessed damage metrics (Fig. 6B – Stimulation) or damage type (Fig. 5C). Functional assessments of SIROF electrode performance (ability to evoke a sensation) also did not correlate with any end-of-study measurements or damage metrics, contrasting with some prior studies [80].

Some explant studies showed significant correlation between electrode metallization damage and stimulation [55]; despite the maximum total charge delivered was only 0.08 mC and implant duration was only 182 days. In our study, electrodes were stimulated up to 8 mC in total and implanted for 956 days, and they showed no such correlation on any array (Fig. 6).

4.6. Explant procedures

One limitation of the comparisons across the three participants is the differences in explant procedures. Given the three different clinical trial locations, the three different neurosurgeons involved, and the uniqueness of each participant's surgical procedures, there existed no protocol from the manufacturer for removal and handling or storage of the arrays. While beyond the scope of this study, it may be beneficial for the manufacturer and other interested parties to develop a standardized explant procedure for device removal, treatment, storage, and end-of-study measurements to assess electrode degradation which may have occurred during implantation.

4.7. Histology

Unlike other analyses of implantations occurring in to-be recessed tissue, the tissue in which these arrays were implanted was healthy and viable, thus not medically justifiable for resection or further analysis. Previous analysis from our group on tissue damage from chronically implanted electrodes in human cortex showed increases in lymphocytic infiltrates, astrogliosis, and foreign body reaction at the implant site, as well as vascular disruption and signs of microhemorrhage from the implant procedure [36]. In all explant surgerical notations, the corresponding neurosurgeons observed the typical impressions left in the cortex after explant (Figure S5), similar to other reports in pre-clinical and clinical studies [55,81,82].

4.8. Implications for brain-computer-interface devices

By evaluating the longevity of implanted electrodes in human cortex, this data may provide valuable insights towards designing the next generation of brain-machine interfaces. Our data suggests Neuroport array micro-electrodes have made important steps towards the goal of a stable electrical interface spanning a multi-decade participant lifetime. Sixty-four (of 96) platinum electrodes were able to record neural action potentials after 0.6 decades of chronic implantation (Fig. 4, AIP(a): SNR). SIROF electrodes improved recording technology even further, showing significantly higher SNR than Platinum (Fig. 8A, SNR). And we observed similarly high stimulation performance, with 61/72 SIROF electrodes able to evoke a sensation, lasting until the end of the implant (Fig. 8B). These significant milestones illustrate the potential of this electrode technology.

However, much work remains to catapult development forward and enable another order of magnitude of electrode longevity. We have identified a new degradation type "pockmarked" which requires further *in vivo* and *in vitro* characterization to fully understand its mechanistic cause and inhibit prevalence on stimulating electrodes (Fig. 6). Despite its higher performance, SIROF electrodes also showed higher degradation than Platinum at equivalent implant durations, suggesting similar electrode lifetimes may not be taken for granted. Our data suggests tip metal of both electrode types is the most susceptible to biotic degradation; the first link in a cascading chain of electrode erosion. Development towards increased tip material resilience may lead to exponential increases in electrode longevity. And as multi-year human clinical trials become more prevalent, clinical standards for explanation, array handling and post-explant electrode characterization are crucial for acquiring the necessary feedback to iterate future electrode design. We hope our methodologies and dataset may provide a blueprint for this work to continue.

Supplemental material

Figure S1 Histogram of degradation metrics (Platinum)

Figure S2 Histogram of degradation metrics (SIROF)
Figure S3 Example failure mechanisms, SEM images
Figure S4 SEM images of each array
Figure S5 Tissue images after explant

Data availability

The data analyzed in this paper will be available upon request.

Funding

David Bjånes: Craig H. Neilson Foundation
Richard Andersen: Tianqiao and Chrissy Chen Brain-machine Interface Center
Boswell Foundation
NIH/NINDS Grant U01NS098975
NIH/NINDS Grant U01NS123127
NIH/NEI R01EY015545
NIH/NEI UG1EY032039
DARPA N66001–10-C-4056
Loren Rieth: DARPA/BTO HAPTIX: N66001–15-C-4017
NIH/NEI: 1UG3NS107688
Francesco Tenore: DARPA HR001120C0120
DARPA N66001–10-C-4056

CRediT authorship contribution statement

David A. Bjånes: Conceptualization, SEM Data Collection, End of Study Data Collection, Investigation, Funding acquisition, Formal analysis, Writing – Original Draft, Writing – Review & Editing. **Spencer Kellis:** Conceptualization, SEM Data Collection, End of Study Data Collection, Investigation, Formal analysis, Writing – Review & Editing. **Robert Nickl:** End of Study Data Collection. **Brian Baker:** SEM Data Collection, Resources. **Tyson Aflalo:** End of Study Data Collection. **Luke Bashford:** End of Study Data Collection. **Srinivas Chivukula:** End of Study Data Collection. **Matthew S. Fifer:** End of Study Data Collection. **Luke E. Osborn:** End of Study Data Collection. **Breanne Christie:** End of Study Data Collection, Writing – Review & Editing. **Brock A. Wester:** End of Study Data Collection. **Pablo A. Celnik:** End of Study Data Collection. **Daniel Kramer:** End of Study Data Collection. **Kelsie Pejsa:** Resources. **Nathan E. Crone:** Clinical. **William S. Anderson:** Clinical. **Nadar Pouratian:** Clinical. **Brian Lee:** Clinical. **Charles Y. Liu:** Clinical, Funding acquisition. **Francesco V. Tenore:** Conceptualization, Resources, Funding acquisition, Writing – Review & Editing. **Loren Rieth:** Conceptualization, SEM Data Collection, Investigation, Resources, Funding acquisition, Writing – Review & Editing. **Richard A. Andersen:** Conceptualization, Resources, Funding acquisition, Writing – Review & Editing.

Declaration of interest statement

The authors declare the following financial interests/personal relationships which may be considered as potential competing interests:

Richard Andersen reports financial support was provided by National Institutes of Health.

Richard Andersen reports financial support was provided by Defense Advanced Research Projects Agency.

Richard Andersen reports financial support was provided by Tianqiao and Chrissy Chen Brain-machine Interface Center.

Richard Andersen reports a relationship with Blackrock Neurotech that includes: funding grants unrelated to this project.

Francesco Tenore reports financial support was provided by Defense Advanced Research Projects Agency.

David Bjanes reports financial support was provided by Craig H Neilsen Foundation.

Richard Andersen reports financial support was provided by James G Boswell Foundation.

Loren Rieth reports financial support was provided by Defense Advanced Research Projects Agency.

Loren Rieth reports financial support was provided by National Institutes of Health.

Nader Pouratian reports a relationship with Boston Scientific and Abbott Laboratories that includes: consulting or advisory.

Spencer Kellis reports a relationship with Blackrock Neurotech that includes: employment.

Loren Rieth reports a relationship with Blackrock Neurotech that includes: funding grants.

If there are other authors, they declare that they have no known competing financial interests or personal relationships that could have appeared to influence the work reported in this paper.

Acknowledgements

The authors would like to thank all the participants for their efforts and engagement in the clinical study. We also thank the clinical staff at Rancho Los Amigos, Casa Colina, USC, UCLA and JHH their work and dedication during the experimental sessions. We would also like thank the staff at the University of Utah and Caltech Imaging Centers for their expertise and assistance imaging the arrays. Big thanks to BSS, JBV, BMG, KK and AS for their assistance scoring the SEM images. This work was developed with variety of funding support for salary, resources, patient care costs, and specialized equipment; including internal research support from the Johns Hopkins University Applied Physics Laboratory (JHU/APL) and funding from the Defense Advanced Research Projects Agency (DARPA) under awards HR001120C0120, N66001–10-C-4056 and N66001–15-C-4017. The views, opinions and/or findings expressed are those of the authors and should not be interpreted as representing the official views or policies of the Department of Defense or the U.S. Government.

Supplementary materials

Supplementary material associated with this article can be found, in the online version, at doi:10.1016/j.actbio.2025.02.030.

References

[1] E.M. Maynard, C.T. Nordhausen, R.A. Normann, The Utah Intracortical Electrode Array: a recording structure for potential brain-computer interfaces, Electroencephalogr. Clin. Neurophysiol. 102 (1997) 228–239, https://doi.org/10.1016/S0013-4694(96)95176-0.
[2] P.R. Kennedy, R.A.E. Bakay, Restoration of neural output from a paralyzed patient by a direct brain connection, Neuroreport 9 (1998) 1707–1711, https://doi.org/10.1097/00001756-199806010-00007.
[3] E.E. Fetz, Real-time control of a robotic arm by neuronal ensembles, Nat. Neurosci. 2 (1999) 583–584, https://doi.org/10.1038/10131.
[4] J. Wessberg, C.R. Stambaugh, J.D. Kralik, P.D. Beck, J.K.Chapin M.Laubach, J. Kim, S.J. Biggs, Real-time prediction of hand tranjectory by ensembles of cortical neurons in primate, Nature 408 (2000) 361–365.
[5] M.D. Serruya, N.G. Hatsopoulos, L. Paninski, M.R. Fellows, J.P. Donoghue, Instant neural control of a movement signal, Nature 416 (2002) 141–142, https://doi.org/10.1038/416141a.
[6] D.M. Taylor, Direct cortical control of 3D neuroprosthetic devices, Science (80-.) 296 (2002) 1829–1832, https://doi.org/10.1126/science.1070291.
[7] M. Velliste, S. Perel, M.C. Spalding, A.S. Whitford, A.B. Schwartz, Cortical control of a prosthetic arm for self-feeding, Nature 453 (2008) 1098–1101, https://doi.org/10.1038/nature06996.
[8] L.R. Hochberg, D. Bacher, B. Jarosiewicz, N.Y. Masse, J.D. Simeral, J. Vogel, S. Haddadin, J. Liu, S.S. Cash, P. van der Smagt, J.P. Donoghue, Reach and grasp by people with tetraplegia using a neurally controlled robotic arm, Nature 485 (2012) 372–375, https://doi.org/10.1038/nature11076.
[9] J.L. Collinger, B. Wodlinger, J.E. Downey, W. Wang, E.C. Tyler-Kabara, D.J. Weber, A.J.C. McMorland, M. Velliste, M.L. Boninger, A.B. Schwartz, High-performance neuroprosthetic control by an individual with tetraplegia, Lancet 381 (2013) 557–564, https://doi.org/10.1016/S0140-6736(12)61816-9.
[10] B. Wodlinger, J.E. Downey, E.C. Tyler-Kabara, A.B. Schwartz, M.L. Boninger, J. L. Collinger, Ten-dimensional anthropomorphic arm control in a human brain−machine interface: difficulties, solutions, and limitations, J. Neural Eng. 12 (2015) 016011, https://doi.org/10.1088/1741-2560/12/1/016011.

[11] R.A. Andersen, T. Aflalo, L. Bashford, D. Bjånes, S. Kellis, Exploring cognition with brain–Machine interfaces, doi:10.1146/Annurev-Psych-030221-030214 73 (2022) 131–158. doi:10.1146/ANNUREV-PSYCH-030221-030214.
[12] S. Musallam, B.D. Corneil, B. Greger, H. Scherberger, R.A. Andersen, Cognitive control signals for neural prosthetics, Science (80-.) 305 (2004) 258–262, https://doi.org/10.1126/science.1097938.
[13] C. Pandarinath, P. Nuyujukian, C.H. Blabe, B.L. Sorice, J. Saab, F.R. Willett, L. R. Hochberg, K.V. Shenoy, J.M. Henderson, High performance communication by people with paralysis using an intracortical brain-computer interface, Elife 6 (2017), https://doi.org/10.7554/ELIFE.18554.
[14] S.K. Wandelt, D.A. Bjånes, K. Pejsa, B. Lee, C. Liu, R.A. Andersen, Online internal speech decoding from single neurons in a human participant, MedRxiv (2022) 2022.11.02.22281775. doi:10.1101/2022.11.02.22281775.
[15] R.A. Normann, E. Fernandez, Clinical applications of penetrating neural interfaces and Utah Electrode Array technologies, J. Neural Eng. 13 (2016) 061003, https://doi.org/10.1088/1741-2560/13/6/061003.
[16] M.A. Salas, L. Bashford, S. Kellis, M. Jafari, H. Jo, D. Kramer, K. Shanfield, K. Pejsa, B. Lee, C.Y. Liu, R.A. Andersen, Proprioceptive and cutaneous sensations in humans elicited by intracortical microstimulation, Elife 7 (2018), https://doi.org/10.7554/eLife.32904.
[17] S.N. Flesher, J.L. Collinger, S.T. Foldes, J.M. Weiss, J.E. Downey, E.C. Tyler-Kabara, S.J. Bensmaia, A.B. Schwartz, M.L. Boninger, R.A. Gaunt, Intracortical microstimulation of human somatosensory cortex, Sci. Transl. Med. 8 (2016) 361ra141, https://doi.org/10.1126/scitranslmed.aaf8083.
[18] M.S. Fifer, D.P. McMullen, L.E. Osborn, T.M. Thomas, B.P. Christie, R.W. Nickl, D. N. Candrea, E.A. Pohlmeyer, M.C. Thompson, M.A. Anaya, W. Schellekens, N. F. Ramsey, S.J. Bensmaia, W.S. Anderson, B.A. Wester, N.E. Crone, P.A. Celnik, G. L. Cantarero, F.V. Tenore, Intracortical somatosensory stimulation to elicit fingertip sensations in an individual with spinal cord injury, Neurology. (2021), https://doi.org/10.1212/wnl.0000000000013173, 10.1212/WNL.0000000000013173.
[19] E. Fernández, A. Alfaro, C. Soto-Sánchez, P. Gonzalez-Lopez, A.M. Lozano, S. Peña, M.D. Grima, A. Rodil, B. Gómez, X. Chen, P.R. Roelfsema, J.D. Rolston, T.S. Davis, R.A. Normann, Visual percepts evoked with an intracortical 96-channel microelectrode array inserted in human occipital cortex, J. Clin. Invest. 131 (2021), https://doi.org/10.1172/JCI151331.
[20] X. Chen, F. Wang, E. Fernandez, P.R. Roelfsema, Shape perception via a high-channel-count neuroprosthesis in monkey visual cortex, Science (80-.) 370 (2020), https://doi.org/10.1126/SCIENCE.ABD7435/SUPPL_FILE/ABD7435S6.MP4.
[21] C.L. Hughes, S.N. Flesher, J.M. Weiss, J.E. Downey, M. Boninger, J.L. Collinger, R. A. Gaunt, Neural stimulation and recording performance in human sensorimotor cortex over 1500 days, J. Neural Eng. 18 (2021), https://doi.org/10.1088/1741-2552/AC18AD.
[22] J.D. Simeral, S.P. Kim, M.J. Black, J.P. Donoghue, L.R. Hochberg, Neural control of cursor trajectory and click by a human with tetraplegia 1000 days after implant of an intracortical microelectrode array, J. Neural Eng. (2011), https://doi.org/10.1088/1741-2560/8/2/025027.
[23] J.E. Downey, N. Schwed, S.M. Chase, A.B. Schwartz, J.L. Collinger, Intracortical recording stability in human brain-computer interface users, J. Neural Eng. 15 (2018), https://doi.org/10.1088/1741-2552/AAB7A0.
[24] X. Chen, F. Wang, R. Kooijmans, P.C. Klink, C. Boehler, M. Asplund, P. R. Roelfsema, Chronic stability of a neuroprosthesis comprising multiple adjacent Utah arrays in monkeys, J. Neural Eng. 20 (2023), https://doi.org/10.1088/1741-2552/ACE07E.
[25] S. Suner, M.R. Fellows, C. Vargas-Irwin, G.K. Nakata, J.P. Donoghue, Reliability of signals from a chronically implanted, silicon-based electrode array in non-human primate primary motor cortex, IEEe Trans. Neural Syst. Rehabil. Eng. 13 (2005) 524–541, https://doi.org/10.1109/TNSRE.2005.857687.
[26] C.A. Chestek, V. Gilja, P. Nuyujukian, J.D. Foster, J.M. Fan, M.T. Kaufman, M. M. Churchland, Z. Rivera-Alvidrez, J.P. Cunningham, S.I. Ryu, K.V. Shenoy, Long-term stability of neural prosthetic control signals from silicon cortical arrays in rhesus macaque motor cortex, J. Neural Eng. 8 (2011), https://doi.org/10.1088/1741-2560/8/4/045005.
[27] J.D. Simeral, S.P. Kim, M.J. Black, J.P. Donoghue, L.R. Hochberg, Neural control of cursor trajectory and click by a human with tetraplegia 1000 days after implant of an intracortical microelectrode array, J. Neural Eng. 8 (2011), https://doi.org/10.1088/1741-2560/8/2/025027.
[28] J.C. Barrese, N. Rao, K. Paroo, C. Triebwasser, C. Vargas-Irwin, L. Franquemont, J. P. Donoghue, Failure mode analysis of silicon-based intracortical microelectrode arrays in non-human primates, J. Neural Eng. 10 (2013), https://doi.org/10.1088/1741-2560/10/6/066014.
[29] J.A. George, D.M. Page, T.S. Davis, C.C. Duncan, D.T. Hutchinson, L.W. Rieth, G. A. Clark, Long-term performance of Utah slanted electrode arrays and intramuscular electromyographic leads implanted chronically in human arm nerves and muscles, J. Neural Eng. 17 (2020) 056042, https://doi.org/10.1088/1741-2552/ABC025.
[30] M.M. Straka, B. Shafer, S. Vasudevan, C. Welle, L. Rieth, Characterizing longitudinal changes in the impedance spectra of In-vivo peripheral nerve electrodes, Micromachines. (Basel) 9 (2018) 587, https://doi.org/10.3390/MI9110587, 2018, Vol. 9, Page 587.
[31] A. Prasad, Q.S. Xue, R. Dieme, V. Sankar, R.C. Mayrand, T. Nishida, W.J. Streit, J. C. Sanchez, Abiotic-biotic characterization of Pt/Ir microelectrode arrays in chronic implants, Front. Neuroeng. 7 (2014) 2, https://doi.org/10.3389/FNENG.2014.00002/BIBTEX.
[32] T.D.Y. Kozai, K. Catt, X. Li, Z.V. Gugel, V.T. Olafsson, A.L. Vazquez, X.T. Cui, Mechanical failure modes of chronically implanted planar silicon-based neural probes for laminar recording, Biomaterials 37 (2015) 25–39, https://doi.org/10.1016/J.BIOMATERIALS.2014.10.040.
[33] K. Woeppel, Q. Yang, X.T. Cui, Recent advances in neural electrode–tissue interfaces, Curr. Opin. Biomed. Eng. 4 (2017) 21–31, https://doi.org/10.1016/J.COBME.2017.09.003.
[34] V.S. Polikov, P.A. Tresco, W.M. Reichert, Response of brain tissue to chronically implanted neural electrodes, J. Neurosci. Methods 148 (2005) 1–18, https://doi.org/10.1016/j.jneumeth.2005.08.015.
[35] J.W. Salatino, K.A. Ludwig, T.D.Y. Kozai, E.K. Purcell, Glial responses to implanted electrodes in the brain, Nat. Biomed. Eng. 1 (2017) 862–877, https://doi.org/10.1038/S41551-017-0154-1.
[36] L.J. Szymanski, S. Kellis, C.Y. Liu, K.T. Jones, R.A. Andersen, D. Commins, B. Lee, D.B. McCreery, C.A. Miller, Neuropathological effects of chronically implanted, intracortical microelectrodes in a tetraplegic patient, J. Neural Eng. 18 (2021) 460–469, https://doi.org/10.1088/1741-2552/ac127e.
[37] A. Woolley, H. Desai, K.O.-J. of neural engineering, undefined 2013, chronic intracortical microelectrode arrays induce non-uniform, depth-related tissue responses, iopscience.Iop.OrgAJ Woolley, HA Desai, KJ OttoJournal Neural Eng. 2013•iopscience.Iop.Org 10 (2013). doi:10.1088/1741-2560/10/2/026007.
[38] J.C. Barrese, J. Aceros, J.P. Donoghue, Scanning electron microscopy of chronically implanted intracortical microelectrode arrays in non-human primates, J. Neural Eng. 13 (2016) 026003, https://doi.org/10.1088/1741-2560/13/2/026003.
[39] C.F. Dunlap, S.C. Colachis, E.C. Meyers, M.A. Bockbrader, D.A. Friedenberg, Classifying intracortical brain-machine interface signal disruptions based on system performance and applicable compensatory strategies: a review, Front. Neurorobot. 14 (2020), https://doi.org/10.3389/FNBOT.2020.558987/FULL.
[40] G. Buzsáki, Large-scale recording of neuronal ensembles, Nat. Neurosci. 7 (2004) 446–451, https://doi.org/10.1038/NN1233.
[41] A.B. Schwartz, X.T. Cui, D.J.J. Weber, D.W. Moran, Brain-controlled interfaces: movement restoration with neural prosthetics, Neuron 52 (2006) 205–220, https://doi.org/10.1016/j.neuron.2006.09.019.
[42] P.J. Rousche, R.A. Normann, Chronic recording capability of the utah intracortical electrode array in cat sensory cortex, J. Neurosci. Methods 82 (1998) 1–15, https://doi.org/10.1016/S0165-0270(98)00031-4.
[43] A. Degenhart, J. Eles, R. Dum, … J.M.-J. of neural, undefined 2016, histological evaluation of a chronically-implanted electrocorticographic electrode grid in a non-human primate, Iopscience.Iop.OrgAD Degenhart, J Eles, R Dum, JL Mischel, I Smalianchuk, B Endler, RC AshmoreJournal Neural Eng. 2016•iopscience.Iop.Org 13 (2016). doi:10.1088/1741-2560/13/4/046019.
[44] E.M. Schmidt, J.S. Mcintosh, M.J. Bak, Long-term implants of Parylene-C coated microelectrodes, Med. Biol. Eng. Comput. 26 (1988) 96–101, https://doi.org/10.1007/BF02441836.
[45] X. Xie, L. Rieth, L. Williams, S. Negi, R. Bhandari, R. Caldwell, R. Sharma, P. Tathireddy, F. Solzbacher, Long-term reliability of Al2O3 and Parylene C bilayer encapsulated Utah electrode array based neural interfaces for chronic implantation, J. Neural Eng. 11 (2014) 9, https://doi.org/10.1088/1741-2560/11/2/026016.
[46] R. Caldwell, M.G. Street, R. Sharma, P. Takmakov, B. Baker, L. Rieth, Characterization of parylene-C degradation mechanisms: in vitro reactive accelerated aging model compared to multiyear in vivo implantation, Biomaterials 232 (2020) 119731, https://doi.org/10.1016/J.BIOMATERIALS.2019.119731.
[47] R. Caldwell, R. Sharma, P. Takmakov, M.G. Street, F. Solzbacher, P. Tathireddy, L. Rieth, Neural electrode resilience against dielectric damage may be improved by use of highly doped silicon as a conductive material, J. Neurosci. Methods 293 (2018) 210–225, https://doi.org/10.1016/J.JNEUMETH.2017.10.002.
[48] P. Ghelich, N.F. Nolta, M. Han, Unprotected sidewalls of implantable silicon-based neural probes and conformal coating as a solution, Npj. Mater. Degrad. 5 (2021), https://doi.org/10.1038/S41529-021-00154-9.
[49] S. Negi, R. Bhandari, L. Rieth, F. Solzbacher, In vitro comparison of sputtered iridium oxide and platinum-coated neural implantable microelectrode arrays, Biomed. Mater. 5 (2010) 15007, https://doi.org/10.1088/1748-6041/5/1/015007.
[50] S. Negi, R. Bhandari, R. Van Wagenen, F. Solzbacher, Factors affecting degradation of sputtered iridium oxide used for neuroprosthetic applications, Proc. IEEe Int. Conf. Micro Electro Mech. Syst. (2010) 568–571, https://doi.org/10.1109/MEMSYS.2010.5442438.
[51] A. Ghazavi, S.F. Cogan, Ultramicro-sized sputtered iridium oxide electrodes in buffered saline: behavior, stability, and the effect of the perimeter to area ratio on their electrochemical properties, Electrochim. Acta 423 (2022) 140514, https://doi.org/10.1016/J.ELECTACTA.2022.140514.
[52] T. Sun, T. Tsaava, J. Peragine, C. Crosfield, M.F. Lopez, R. Modi, R. Sharma, C. Li, H. Sohal, E.H. Chang, L. Rieth, Flexible IrOx neural electrode for mouse vagus nerve stimulation, Acta Biomater. 159 (2023) 394–409, https://doi.org/10.1016/J.ACTBIO.2023.01.026.
[53] S.F. Cogan, Neural stimulation and recording electrodes, Annu Rev. Biomed. Eng. 10 (2008) 275–309, https://doi.org/10.1146/annurev.bioeng.10.061807.160518.
[54] P.J. Gilgunn, X.C. Ong, S.N. Flesher, A.B. Schwartz, R.A. Gaunt, Structural analysis of explanted microelectrode arrays, in: Int. IEEE/EMBS Conf. Neural Eng. NER, 2013, pp. 719–722, https://doi.org/10.1109/NER.2013.6696035.
[55] K. Woeppel, C. Hughes, A.J. Herrera, J.R. Eles, E.C. Tyler-Kabara, R.A. Gaunt, J. L. Collinger, X.T. Cui, Explant analysis of Utah electrode arrays implanted in Human cortex for brain-computer-interfaces, Front. Bioeng. Biotechnol. 9 (2021) 1137, https://doi.org/10.3389/FBIOE.2021.759711/BIBTEX.
[56] P. Takmakov, K. Ruda, K. Scott Phillips, I.S. Isayeva, V. Krauthamer, C.G. Welle, Rapid evaluation of the durability of cortical neural implants using accelerated

aging with reactive oxygen species, J. Neural Eng. 12 (2015), https://doi.org/10.1088/1741-2560/12/2/026003.
[57] M.G. Street, C.G. Welle, P.A. Takmakov, Automated reactive accelerated aging for rapid in vitro evaluation of neural implant performance, Rev. Sci. Instrum. 89 (2018), https://doi.org/10.1063/1.5024686.
[58] A. Prasad, Q.S. Xue, V. Sankar, T. Nishida, G. Shaw, W.J. Streit, J.C. Sanchez, Comprehensive characterization and failure modes of tungsten microwire arrays in chronic neural implants, J. Neural Eng. 9 (2012), https://doi.org/10.1088/1741-2560/9/5/056015.
[59] A. Prasad, J.C. Sanchez, Quantifying long-term microelectrode array functionality using chronic in vivo impedance testing, J. Neural Eng. 9 (2012), https://doi.org/10.1088/1741-2560/9/2/026028.
[60] C. Bennett, M. Samikkannu, F. Mohammed, W.D. Dietrich, S.M. Rajguru, A. Prasad, Blood brain barrier (BBB)-disruption in intracortical silicon microelectrode implants, Biomaterials 164 (2018) 1–10, https://doi.org/10.1016/j.biomaterials.2018.02.036.
[61] C. Bennett, F. Mohammed, A. Álvarez-Ciara, M.A. Nguyen, W.D. Dietrich, S. M. Rajguru, W.J. Streit, A. Prasad, Neuroinflammation, oxidative stress, and blood-brain barrier (BBB) disruption in acute Utah electrode array implants and the effect of deferoxamine as an iron chelator on acute foreign body response, Biomaterials 188 (2019) 144–159, https://doi.org/10.1016/J.BIOMATERIALS.2018.09.040.
[62] S. Negi, R. Bhandari, L. Rieth, F. Solzbacher, In vitro comparison of sputtered iridium oxide and platinum-coated neural implantable microelectrode arrays, Biomed. Mater. 5 (2010) 15007, https://doi.org/10.1088/1748-6041/5/1/015007.
[63] T. Aflalo, S. Kellis, C. Klaes, B. Lee, Y. Shi, K. Pejsa, K. Shanfield, S. Hayes-Jackson, M. Aisen, C. Heck, C. Liu, R.A. Andersen, Decoding motor imagery from the posterior parietal cortex of a tetraplegic human, Science 348 (2015) 906–910, https://doi.org/10.1126/science.aaa5417.
[64] T. Aflalo, C. Zhang, B. Revechkis, E. Rosario, N. Pouratian, R.A. Andersen, Implicit mechanisms of intention, Curr. Biol. 32 (2022) 2051–2060, https://doi.org/10.1016/J.CUB.2022.03.047, e6.
[65] A.T. Gardner, H.J. Strathman, D.J. Warren, R.M. Walker, Impedance and noise characterizations of Utah and microwire electrode arrays, IEEE J. Electromagn. RF Microwaves Med. Biol. 2 (2018) 234–241, https://doi.org/10.1109/JERM.2018.2862417.
[66] T. Chai, R.R. Draxler, Root mean square error (RMSE) or mean absolute error (MAE)?-arguments against avoiding RMSE in the literature, Geosci. Model. Dev. 7 (2014) 1247–1250, https://doi.org/10.5194/gmd-7-1247-2014.
[67] A.T. Rajan, J.L. Boback, J.F. Dammann, F.V. Tenore, B.A. Wester, K.J. Otto, R. A. Gaunt, S.J. Bensmaia, The effects of chronic intracortical microstimulation on neural tissue and fine motor behavior, J. Neural Eng. 12 (2015), https://doi.org/10.1088/1741-2560/12/6/066018.
[68] M.S. Fifer, D.P. McMullen, T.M. Thomas, L.E. Osborn, R.W. Nickl, D.N. Candrea, E. A. Pohlmeyer, M.C. Thompson, M. Anaya, W. Schellekens, N.F. Ramsey, S.J. Bensmaia, W.S. Anderson, B.A. Wester, N.E. Crone, P.A. Celnik, G.L. Cantarero, F. V. Tenore, Intracortical microstimulation elicits Human fingertip sensations, MedRxiv (2020) 2020.05.29.20117374. doi:10.1101/2020.05.29.20117374.
[69] L.E. Osborn, D.P. McMullen, B.P. Christie, P. Kudela, T.M. Thomas, M. C. Thompson, R.W. Nickl, M. Anaya, S. Srihari, N.E. Crone, B.A. Wester, P. A. Celnik, G.L. Cantarero, F.V. Tenore, M.S. Fifer, Intracortical microstimulation of somatosensory cortex generates evoked responses in motor cortex, in: Int. IEEE/EMBS Conf. Neural Eng. NER 2021-May, 2021, pp. 53–56, https://doi.org/10.1109/NER49283.2021.9441123.
[70] B. Christie, L.E. Osborn, D.P. McMullen, A.S. Pawar, T.M. Thomas, S.J. Bensmaia, P.A. Celnik, M.S. Fifer, F.V. Tenore, Perceived timing of cutaneous vibration and intracortical microstimulation of human somatosensory cortex, Brain Stimul. 15 (2022) 881–888, https://doi.org/10.1016/J.BRS.2022.05.015.
[71] P.A.P. Moran, Notes on continuous stochastic phenomena, Biometrika 37 (1950) 17, https://doi.org/10.2307/2332142.
[72] K.A. Sillay, P. Rutecki, K. Cicora, G. Worrell, J. Drazkowski, J.J. Shih, A.D. Sharan, M.J. Morrell, J. Williams, B. Wingeier, Long-term measurement of impedance in chronically implanted depth and subdural electrodes during responsive neurostimulation in humans, Brain Stimul. 6 (2013) 718–726, https://doi.org/10.1016/J.BRS.2013.02.001.
[73] S.A. Jones, S.-H. Shim, J. He, X. Zhuang, Fast, three-dimensional super-resolution imaging of live cells, Nat. Methods 8 (2011) 499–505, https://doi.org/10.1038/nmeth.1605.
[74] V. Thakore, P. Molnar, J.J. Hickman, An optimization-based study of equivalent circuit models for representing recordings at the neuron-electrode interface, IEEE Trans. Biomed. Eng. 59 (2012) 2338–2347, https://doi.org/10.1109/TBME.2012.2203820.
[75] N. Lago, A. Cester, N. Wrachien, M. Natali, S.D. Quiroga, S. Bonetti, M. Barbato, A. Rizzo, E. Benvenuti, V. Benfenati, M. Muccini, S. Toffanin, G. Meneghesso, A physical-based equivalent circuit model for an organic/electrolyte interface, Org. Electron. 35 (2016) 176–185, https://doi.org/10.1016/J.ORGEL.2016.05.018.
[76] J. Jiang, F.R. Willett, D.M. Taylor, Relationship between microelectrode array impedance and chronic recording quality of single units and local field potentials, in: 2014 36th Annu. Int. Conf. IEEE Eng. Med. Biol. Soc. EMBC 2014, 2014, pp. 3045–3048, https://doi.org/10.1109/EMBC.2014.6944265.
[77] P.A. Cody, J.R. Eles, C.F. Lagenaur, T.D.Y. Kozai, X.T. Cui, Unique electrophysiological and impedance signatures between encapsulation types: an analysis of biological Utah array failure and benefit of a biomimetic coating in a rat model, Biomaterials 161 (2018) 117–128, https://doi.org/10.1016/J.BIOMATERIALS.2018.01.025.
[78] S.W… Freiman, J.J… Mecholsky, The Fracture of Brittle Materials: Testing and Analysis, John Wiley & Sons, Inc., 2012, https://doi.org/10.1002/9781118147757.
[79] E. Ilic, A. Pardo, R. Hauert, P. Schmutz, S. Mischler, Silicon corrosion in neutral Media: the influence of confined geometries and crevice corrosion in simulated physiological solutions, J. Electrochem. Soc. 166 (2019) C125–C133, https://doi.org/10.1149/2.0241906JES/XML.
[80] S.R. Kane, S.F. Cogan, J. Ehrlich, T.D. Plante, D.B. McCreery, P.R. Troyk, Electrical performance of penetrating microelectrodes chronically implanted in cat cortex, IEEE Trans. Biomed. Eng. 60 (2013) 2153–2160, https://doi.org/10.1109/TBME.2013.2248152.
[81] P.A. House, J.D. MacDonald, P.A. Tresco, R.A. Normann, Acute microelectrode array implantation into human neocortex: preliminary technique and histological considerations, Neurosurg. Focus. 20 (2006), https://doi.org/10.3171/FOC.2006.20.5.5.
[82] B.P. Christie, K.R. Ashmont, P.A. House, B. Greger, Approaches to a cortical vision prosthesis: implications of electrode size and placement, J. Neural Eng. 13 (2016), https://doi.org/10.1088/1741-2560/13/2/025003.